Early zygotic gene product Dunk interacts with anillin to regulate Myosin II during *Drosophila* cleavage

Jiayang Chen[a], Andreia F. Verissimo[b], Angela R. Kull[b], and Bing He[a,*]
[a]Department of Biological Sciences, Dartmouth College, Hanover, NH 03755; [b]Institute for Biomolecular Targeting (bioMT), Geisel School of Medicine at Dartmouth, Hanover, NH 03755

ABSTRACT ***Drosophila melanogaster* cellularization is a special form of cleavage that converts syncytial embryos into cellular blastoderms by partitioning the peripherally localized nuclei into individual cells. An early event in cellularization is the recruitment of nonmuscle myosin II ("myosin") to the leading edge of cleavage furrows, where myosin forms an interconnected basal array before reorganizing into individual cytokinetic rings. The initial recruitment and organization of basal myosin are regulated by a cellularization-specific gene, *dunk*, but the underlying mechanism is unclear. Through a genome-wide yeast two-hybrid screen, we identified anillin (Scraps in *Drosophila*), a conserved scaffolding protein in cytokinesis, as the primary binding partner of Dunk. Dunk colocalizes with anillin and regulates its cortical localization during the formation of cleavage furrows, while the localization of Dunk is independent of anillin. Furthermore, Dunk genetically interacts with anillin to regulate the basal myosin array during cellularization. Similar to Dunk, anillin colocalizes with myosin since the very early stage of cellularization and is required for myosin retention at the basal array, before the well-documented function of anillin in regulating cytokinetic ring assembly. Based on these results, we propose that Dunk regulates myosin recruitment and spatial organization during early cellularization by interacting with and regulating anillin.**

SIGNIFICANCE STATEMENT

- During *Drosophila* cellularization, a special cleavage, the recruitment of non-muscle myosin II to the cleavage furrows is regulated by a cellularization-specific gene, but the underlying mechanism is unclear.
- Through a genome-wide yeast two-hybrid screen, the authors identified the conserved cytokinesis protein anillin as the primary Dunk binding partner. The authors further demonstrate that Dunk regulates myosin through anillin during early cellularization.
- These findings have uncovered a previously unappreciated function of anillin in the early stage of a cytokinetic process and shed light on how conserved cytokinetic machinery can be adapted in evolution to achieve a special form of cytokinesis.

Monitoring Editor
Richard Fehon
University of Chicago

Received: Feb 15, 2022
Revised: Jul 5, 2023
Accepted: Jul 19, 2023

This article was published online ahead of print in MBoC in Press (http://www.molbiolcell.org/cgi/doi/10.1091/mbc.E22-02-0046).

Author contributions: B.H. and J.C designed the study. J.C. performed the yeast two-hybrid screen. A.F.V. and A.R.K. performed protein expression in the insect expression system for the in vitro binding experiment. J.C. and B.H. performed the rest of the experiments, analyzed the data, and wrote the manuscript.

*Address correspondence to: Bing He (bing.he@dartmouth.edu).

Abbreviations used: ABD, actin binding domain; AH, anillin homology; Bnk, bottleneck; MBD, myosin binding domain; PH, Pleckstrin homology; Pnut, Peanut; Sqh, Spaghetti squash.

INTRODUCTION

Cytokinesis, which partitions the cellular contents of one dividing cell into two daughter cells following mitosis or meiosis, is one of the most critical events for living organisms (Rappaport, 1971; Green *et al.*, 2012). As cytokinesis starts, a contractile ring composed of F-actin and nonmuscle myosin II (hereafter referred to as "myosin") forms at the cell equator. The subsequent constriction of this ring drives cleavage furrow invagination and eventually pinches off the two daughter cells (Eggert *et al.*, 2006; Green *et al.*, 2012). The tight regulation of myosin activity, organization, and localization enables the proper constriction and separation of the daughter cells (Green *et al.*, 2012; Pollard and O'Shaughnessy, 2019). In this study, we sought to understand how cells utilized the conserved cytokinesis machinery to achieve a special form of cleavage.

Drosophila melanogaster cellularization is an atypical form of cytokinesis that mediates cellular blastoderm formation during early *Drosophila* embryogenesis (Mazumdar and Mazumdar, 2002). Before cellularization, the *Drosophila* embryo undergoes 13 rounds of nuclear division without cytokinesis, generating a syncytial blastoderm with ~ 6000 nuclei aligned near the surface of the embryo (Foe and Alberts, 1983). At the onset of cellularization, the plasma membrane begins to invaginate and form cleavage furrows between the syncytial nuclei. Approximately an hour later, a monolayer of epithelial cells forms at the peripheral region of the embryo, marking the end of cellularization (Mazumdar and Mazumdar, 2002; Sokac *et al.*, 2023). Similar to conventional cytokinesis, active myosin is recruited to the cell cortex at the onset of the cellularization and becomes concentrated at the leading edge of nascent cleavage furrows, also known as "cellularization front" or "furrow canals" (Figure 1A; Fullilove and Jacobson, 1971; Royou *et al.*, 2004). This initial recruitment of myosin is associated with a cortical flow of punctum-like apical myosin structures toward the nascent furrows (He *et al.*, 2016). This initial, flow-associated recruitment is followed by direct recruitment of myosin from the cytoplasm to the furrow tip (Royou *et al.*, 2004; He *et al.*, 2016). Myosin recruited to the cellularization front first organizes into an interconnected hexagonal array that resembles the spatial pattern of the ingressing furrows. Approximately 30 min into cellularization, this basal myosin array reorganizes into individual myosin rings, which contract and eventually close off the base of the newly formed cells ("basal closure"; Figure 1A; Royou *et al.*, 2004; Xue and Sokac, 2016). In addition to myosin, many other structural components and regulators of the cytokinetic ring are shared between cellularization and conventional animal cytokinesis, such as actin (Schejter and Wieschaus, 1993), RhoA (Rho1 in *Drosophila*) and its regulators (Crawford *et al.*, 1998; Grosshans *et al.*, 2005; Barmchi *et al.*, 2005; Wenzl *et al.*, 2010; Mason *et al.*, 2016; Sharma and Rikhy, 2021), anillin (Scraps in *Drosophila*; Field and Alberts, 1995; Field *et al.*, 2005), septin (Adam *et al.*, 2000; Field *et al.*, 2005), and the formin protein Diaphanous (Afshar *et al.*, 2000; Grosshans *et al.*, 2005). These conserved cytokinetic components are mainly maternally provided, many of which are involved in regulating the localization and function of myosin during cellularization.

In addition to the conserved cytokinetic factors, a small number of "cellularization-specific" genes are also involved in regulating cellularization. Five of such "cellularization genes" have been identified as follows: *nullo*, *serendipity-α*, *bottleneck (bnk)*, *slam*, and *dunk* (Merrill *et al.*, 1988; Wieschaus and Sweeton, 1988; Schweisguth *et al.*, 1990; Rose and Wieschaus, 1992; Schejter and Wieschaus, 1993; Lecuit *et al.*, 2002; He *et al.*, 2016). The transition from the syncytial stage to cellularization is preceded by the massive induction of zygotic gene expression in the embryo (Renzis *et al.*, 2007; Liang *et al.*, 2008; Tadros and Lipshitz, 2009). The five cellularization genes are all expressed in a short time window around the onset of cellularization, and the corresponding proteins rapidly disappear during late cellularization. The products of these genes are all localized to the furrow canals and are involved in regulating the basal actin–myosin (actomyosin) structures, either directly or indirectly. Dunk is critical for the flow phase of myosin recruitment during the first 10 min of cellularization (He *et al.*, 2016). Slam, on the other hand, is important for the subsequent, direct recruitment of myosin to the cellularization front (Lecuit *et al.*, 2002; Wenzl *et al.*, 2010; Acharya *et al.*, 2014; He *et al.*, 2016). Nullo and Serendipity-α promote actin assembly at the furrow canals, supporting actomyosin contractility and preventing degeneration of cleavage furrows (Schweisguth *et al.*, 1990; Rose and Wieschaus, 1992; Sokac and Wieschaus, 2008; Zheng *et al.*, 2013). Finally, Bnk acts as an actin-crosslinking protein that functions to dampen actomyosin contractility and restrain the transition from basal myosin network into individual myosin rings, thereby ensuring the proper timing of basal closure (Schejter and Wieschaus, 1993; Reversi *et al.*, 2014; Krueger *et al.*, 2019). While the molecular functions of several cellularization proteins have started to be elucidated, how Dunk regulates myosin during cellularization remains elusive.

Anillin is a highly conserved protein that plays an important role during cytokinesis (Field and Alberts, 1995; Piekny and Maddox, 2010) and has recently been implicated in the development of various cancers (Shimizu *et al.*, 2007; Naydenov *et al.*, 2020; Cui *et al.*, 2022; Zhang *et al.*, 2023). The structure of anillin is well defined, revealing multiple protein–protein interaction domains conserved throughout species from *Drosophila* to humans (Piekny and Maddox, 2010). Anillin binds to the actomyosin network through its myosin- and actin-binding domains (MBD and ABD, respectively) at its N-terminus and links the contractile ring to the cell membrane through the anillin homology (AH) domain and a Pleckstrin homology (PH) domain at its C-terminus (Figure 1B; Piekny and Glotzer, 2008; Liu *et al.*, 2012; Sun *et al.*, 2015; Budnar *et al.*, 2019). Anillin's regulators RhoA and $PI(4,5)P_2$ bind to the AH domain of anillin and facilitate its cortical localization (Piekny and Glotzer, 2008; Liu *et al.*, 2012; Sun *et al.*, 2015; Budnar *et al.*, 2019). The PH domain of anillin synergizes with the AH domain to promote membrane association and is required for the proper cortical localization of anillin (Piekny and Glotzer, 2008; Liu *et al.*, 2012; Sun *et al.*, 2015). The PH domain of anillin binds to the septin subunit Peanut (Pnut; Field *et al.*, 2005; Liu *et al.*, 2012). Although the septin cytoskeleton provides important structural functions required for the completion of cytokinesis, it is dispensable for the membrane localization of anillin (Field *et al.*, 2005; Liu *et al.*, 2012). During conventional animal cytokinesis, anillin functions to promote the temporal and spatial stability of the actomyosin network at the cell equator and facilitate the organization of actomyosin into contractile rings (Piekny and Maddox, 2010). For example, in HeLa cells, the loss of anillin leads to destabilization and oscillation of the actomyosin ring around the equatorial region (Piekny and Glotzer, 2008). During *Drosophila* cellularization, loss of anillin leads to disorganization of basal actomyosin rings and failure in basal closure (Thomas and Wieschaus, 2004; Field *et al.*, 2005). In both cases, however, myosin is still recruited to the cleavage furrows and is able to contract (Thomas and Wieschaus, 2004; Field *et al.*, 2005; Piekny and Glotzer, 2008). The lack of obvious phenotype in initial myosin recruitment upon disruption of anillin may be due to functional redundancy, as suggested by studies in cultured cells (Piekny and Glotzer, 2008). In addition to a critical function in cytokinesis, recent studies have also revealed anillin's function in regulating myosin localization at the cell–cell junctions (Wang *et al.*, 2015) and organizing medial–apical actomyosin network in nondividing

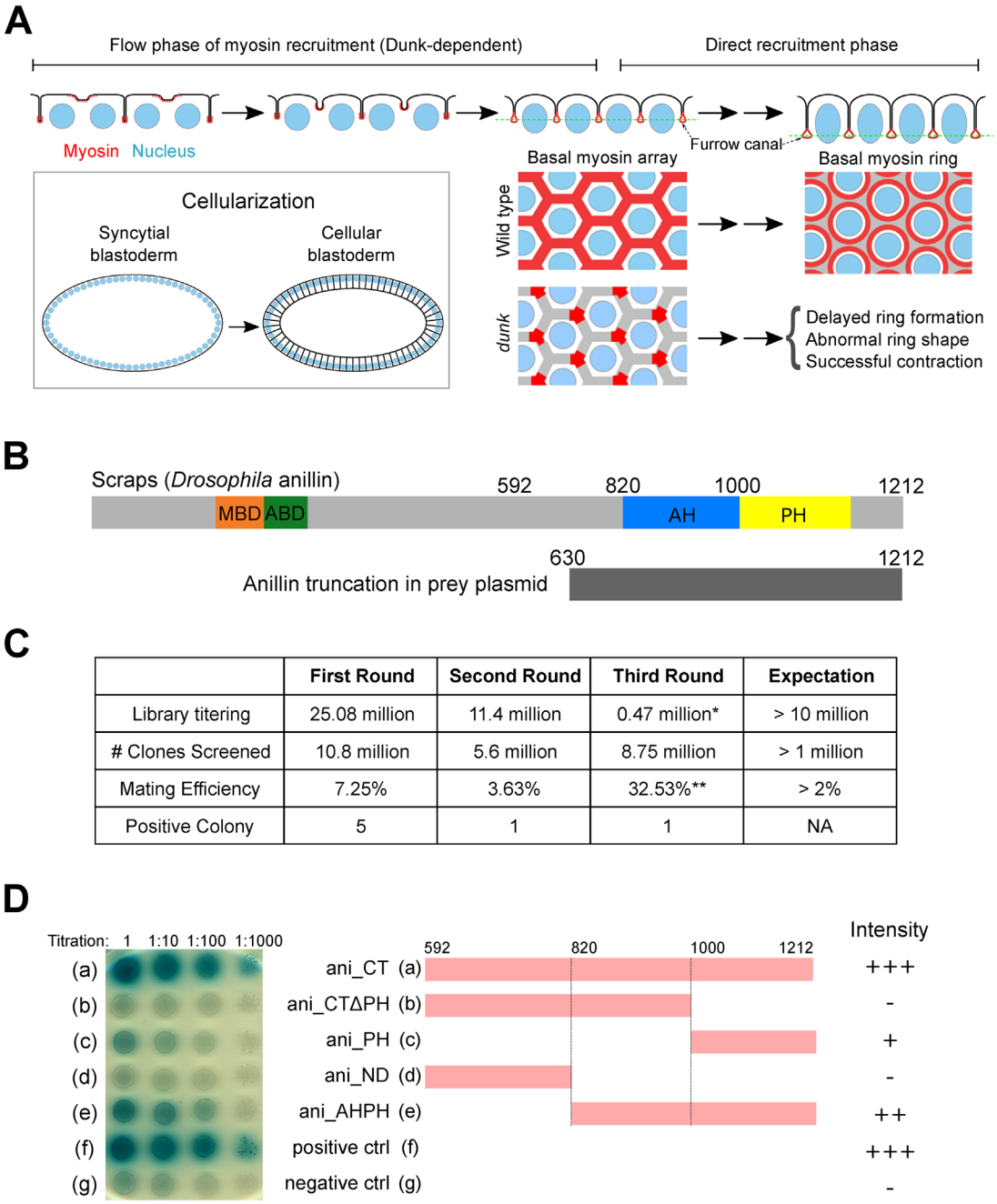

	First Round	Second Round	Third Round	Expectation
Library titering	25.08 million	11.4 million	0.47 million*	> 10 million
# Clones Screened	10.8 million	5.6 million	8.75 million	> 1 million
Mating Efficiency	7.25%	3.63%	32.53%**	> 2%
Positive Colony	5	1	1	NA

FIGURE 1: Dunk interacts with the C-terminal region of anillin. (A) Schematics showing myosin recruitment to the cleavage furrows during *Drosophila* cellularization and the basal myosin phenotype in *dunk* mutant embryos. (B) Top: domain structure of Scraps, the *Drosophila* anillin. The C-terminal region of anillin is the sole Dunk interactor identified in our yeast two-hybrid screen. Bottom: the schema of the truncated anillin protein encoded by the anillin sequence in the prey library. The information on anillin truncation was obtained by sequencing the prey plasmids from the positive colonies. All seven positive colonies were sequenced, and all started around 630 a.a. of the full-length anillin. (C) A table showing the library titering, numbers of clones screened, mating efficiency, and the number of positive clones for each repeat. The library titering indicates whether the library is healthy enough and contains enough yeast cells; the number of clones screened is the indicator of the number of yeast cells from the library that have been gone through each screen; mating efficiency indicates whether bait cell and prey cell mated successfully (Mate & Plate Library - Universal *Drosophila* [Normalized], Takara, catalogue no. 630485). The unexpected and abnormal titering (*) and matting efficiency (**) of the third round of repeats have resulted from the low number of colonies growing on the SD/-Leu control plate (See *Materials and Methods* for details). (D) Left: one representative DDO/–Leu/–Trp/X-alpha-Gal agar plate showing the growth and color reaction of yeast cells for each pair of bait and prey. (a): Dunk with full-length C-terminal anillin (ani_CT), 592–1212 a.a.; (b): Dunk with AH domain (ani_CTΔPH), 592–999 a.a.; (c): Dunk with PH domain (ani_PH), 1000–1212 a.a.; (d): Dunk with C-terminal region without AH domain and PH domain (ani_ND), 592–819 a.a.; (e): Dunk with AH domain and the PH domain (ani_AHPH), 820–1212 a.a.; (f): positive control (p53 with T-antigen); and (g): negative control (Lam with T-antigen). Right: a schematic outlining the constructs used for pairwise yeast two-hybrid assay.

epithelial cells (Arnold *et al.*, 2019). Interestingly, a recent study suggests that anillin may function as an unconventional RhoA effector that feeds back and boosts RhoA's activity by kinetically increasing its residence time at $PI(4,5)P_2$-enriched membrane (Budnar *et al.*, 2019). How the functions of anillin in regulating cellular contractility are involved in an early stage of cytokinesis before the formation of the cytokinetic ring is not fully understood.

Here, we report the identification of anillin as a Dunk binding partner in a genome-wide yeast two-hybrid screen and provide evidence that Dunk and anillin function together to regulate cortical myosin during early cellularization. We show that Dunk colocalizes with anillin during early cellularization and regulates the initial recruitment of anillin during the formation of cleavage furrows. In the absence of Dunk, anillin and the septin subunit Pnut show aberrant localization at the cellularization front. In contrast, Dunk's cortical localization does not require anillin. We further show that *dunk* and *anillin* genetically interact with each other, and they display similar synthetic effects on basal myosin organization when combined with the loss of Bnk. Finally, we show that anillin colocalizes with myosin at the cellularization front throughout the formation and extension of the cleavage furrows. Disruption of the function of anillin impairs the initial recruitment of myosin to the incipient cleavage furrows and causes aberrant myosin distribution at the cellularization front that closely resembles the basal myosin phenotype in the *dunk* mutant. Taken together, our results suggest that Dunk regulates myosin recruitment and organization during early cellularization by interacting with and regulating anillin.

RESULTS

Identification of anillin as a binding partner for Dunk

Previous study has shown that the zygotic gene *dunk* functions to facilitate the flow phase of myosin recruitment during early cellularization. In *dunk* mutant embryos, myosin is progressively depleted from the cellularization front during the first 5–10 min of cellularization, resulting in a fragmented basal myosin array with a low level of myosin at most edges of the hexagonal array (Figure 1A; He *et al.*, 2016). Dunk is a small protein (246 amino acids [a.a.]) with no previously identified homologue or well-characterized structure motifs. To understand how Dunk regulates myosin in cellularization, we performed a genome-wide yeast two-hybrid screen to identify Dunk binding partners. We used full-length Dunk protein as the bait to screen a normalized *Drosophila* cDNA library (Mate & Plate Library - Universal *Drosophila* [Normalized], Takara, catalogue no. 630485). This library was prepared from a mix of equal quantities of poly-A+ RNAs isolated from the embryo, larva, and adult-stage *Drosophila* and covers most of the expressed genes. Scraps, the *Drosophila* homologue of anillin, was the only protein that displayed positive interaction with Dunk in the three repeats of the screen (Figure 1, B and C). Of note, the cDNAs in the library on average cover ≤ 600 a.a. from the C-terminus of the encoded prey proteins (Pretransformed Mate & Plate Libraries [January 2008] Clontechniques XXIV(1):26–27). For example, it only contains the last 583 a.a. (630–1212 a.a.) from the C-terminus of anillin (Figure 1B). It is, therefore, possible that we have missed the binding partner of Dunk that is longer than 600 a.a. and requires its N-terminal portion to bind to Dunk. On the other hand, the result that anillin is the only binding protein identified in the screen suggests that the bait protein in the assay was not "sticky." Therefore, the interaction we detected was unlikely due to nonspecific binding.

Next, we sought to use yeast two-hybrid to confirm the result from the screen and further determine the minimal region of anillin that binds to Dunk. Anillin is a multidomain scaffold protein that binds to the actomyosin network through its N-terminal MBD and ABD and to the cell membrane through its C-terminal domains (Piekny and Maddox, 2010; Figure 1B). The C-terminal portion of anillin is important for its cortical localization and is well conserved from *Drosophila* to humans (Field *et al.*, 2005; Piekny and Maddox, 2010; Sun *et al.*, 2015). The positive clones identified in our screen all contain the C-terminal portion of anillin, which includes the conserved AH and PH domains (Figure 1B). We generated prey constructs of different truncations of anillin and tested for the interaction with Dunk as the bait in a pairwise yeast two-hybrid assay (Figure 1D; Supplemental Figure S1). The prey construct containing the entire C-terminal region of anillin ("ani_CT", 592–1212 a.a.) showed the strongest interaction with Dunk (Figure 1D, "a"). A truncated fragment containing both the AH and PH domains ("ani_AHPH", 820–1212 a.a.) also showed positive interaction with Dunk, albeit weaker compared with ani_CT (Figure 1D, "e"). Removing the AH domain from ani_AHPH ("ani_PH", 1000–1212 a.a.) further reduced the binding affinity, although a weak interaction could still be detected (Figure 1D, "c"). In contrast, removing the PH domain from the C-terminal region of anillin completely abolished the interaction (Figure 1D, "b" and "d"). These results suggest that the AH and PH domains of anillin (and to a lesser extent the PH domain) can mediate a weak interaction with Dunk, but the sequence outside of the AH and PH domains also substantially contributes to Dunk–anillin interaction. Together, the results of the pairwise yeast two-hybrid assay confirmed the finding from the genome-wide screen and further mapped the Dunk binding site on anillin to a region encompassing the conserved AH and PH domains.

We have employed several approaches to test the biochemical interaction between Dunk and anillin. However, these tests were unsuccessful due to various technical challenges. Our attempts to confirm the interaction by immunoprecipitation were hindered by difficulties in detecting Dunk proteins in embryo lysates. In addition, we found that Dunk was largely insoluble in several protein expression systems we tested, preventing us from testing the interaction by in vitro binding assays using purified recombinant proteins (See *Supplemental Notes* for details). Thus, it remains to be tested in the future whether Dunk and anillin directly interact with each other and whether this interaction occurs in cellularizing embryos.

Dunk colocalizes with anillin during cellularization

Anillin is a well-conserved regulator for cytokinesis that interacts with the actomyosin ring. In light of the previous finding that Dunk regulates myosin recruitment during the formation of basal myosin array in early cellularization (He *et al.*, 2016), we hypothesized that Dunk regulates myosin through interacting with anillin. To test this hypothesis, we first investigated whether Dunk colocalizes with anillin during cellularization. To this end, we generated an endogenously tagged anillin-mCherry line using the CRISPR/Cas9 technique (See *Methods*) and examined the localization of Dunk and anillin by immunofluorescence using the Dunk and mCherry antibodies. For each embryo, we measured the length of cleavage furrows to indicate its stage during cellularization (Figure 2, yellow line in the cross-sectional view). At the very early stage of cellularization, Dunk and anillin colocalize with each other at the rim of the apical cap above the newly formed daughter nucleus (Figure 2, "Onset cellularization"). At a slightly later stage, the rim of the neighboring cap appeared to fuse to each other as furrow ingression proceeded, forming an interconnected basal hexagonal array at the leading edge of the furrows (Figure 2, "Early cellularization"). Dunk and anillin uniformly decorated this basal array and remained colocalized when individual cytokinetic rings started to form (Figure 2, "Early cellularization" to "Mid cellularization"). Together, these observations demonstrate that Dunk and anillin colocalize with each other at the leading edge of the cleavage furrows.

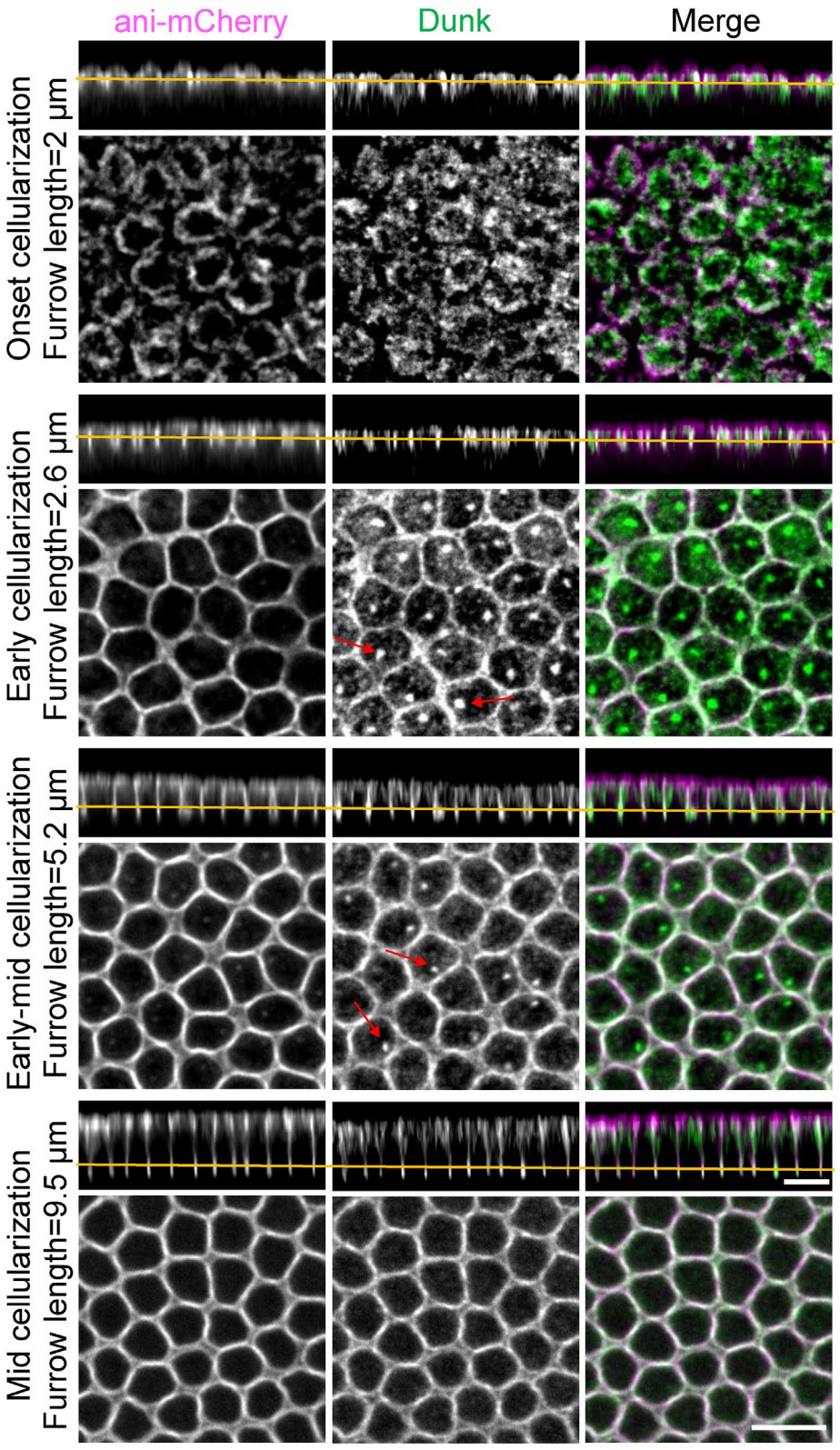

FIGURE 2: Localization of Dunk and anillin during early and midcellularization. The immunofluorescence staining images of anillin-mCherry (ani-mCherry, endogenously tagged) embryos stained with mCherry and Dunk antibodies. Upper panels: cross-sectional views, generated by reslicing of confocal z-stacks; bottom panels: en face view, maximum projections of 2–3-µm confocal sections covering the furrow canals; yellow lines: cellularization front. The intensities of the en face views have been individually adjusted, making the intensity comparable between two protein signals and between different timepoints, to better demonstrate the colocalization of the two proteins. Dunk and anillin started to show partial colocalization at the rim structure above each newly formed daughter nucleus ("onset cellularization"). The colocalization becomes more extensive after the rim fused to each other and formed an interconnected basal array at the leading edge of the furrows. The two proteins remained colocalized at the basal array and when the basal array reorganizes into individual rings. Red arrows indicate an unknown punctum-like structure caused by nonspecific staining by the anti-Dunk antibody, which we also observed in *dunk* mutant embryos (unpublished data). All scale bars: 10 µm.

Dunk regulates the spatial distribution of anillin at the cellularization front

Because Dunk and anillin colocalize at the cellularization front, we next asked whether Dunk regulates the localization of anillin during cellularization. Previous studies have shown that anillin is concentrated at the cellularization front and colocalizes with the basal actomyosin rings (Field et al, 2005). We examined anillin localization in wild-type and *dunk* mutant embryos by immunofluorescence. Our results revealed that in *dunk* mutant embryos, anillin was still recruited to the furrow canals, but the spatial distribution of anillin at the furrow canals was abnormal (Figure 3A). During early cellularization, anillin was evenly distributed across the cellularization front in wild-type embryos, forming an interconnected hexagonal array that was analogous to the basal myosin array. In *dunk* mutant embryos, however, the distribution of anillin at the basal array was less homogeneous compared with the wild type (Figure 3A, green and magenta arrows show enrichment and depletion of the anillin signal, respectively). By the time anillin started to reorganize into individual rings in wild-type embryos (Figure 3A, Early–mid cellularization), the anillin signal in *dunk* mutant embryos became more homogeneous across the leading edge, suggesting a partial recovery from the early defect (Figure 3A, Early–mid cellularization). However, in contrast to the wild-type embryo where anillin was enriched in curved bundles that resemble part of the cytokinetic rings (Figure 3A, yellow arrows), there was no sign of contractile ring formation in *dunk* mutant embryos (Figure 3A, Early–mid cellularization). By the time anillin clearly formed discrete rings in wild-type embryos (Figure 3A, "Mid cellularization" and "Mid–late cellularization", yellow arrowheads), anillin in *dunk* mutant appeared to just start to rearrange into individual rings. The shape of these rings was irregular, and the neighboring

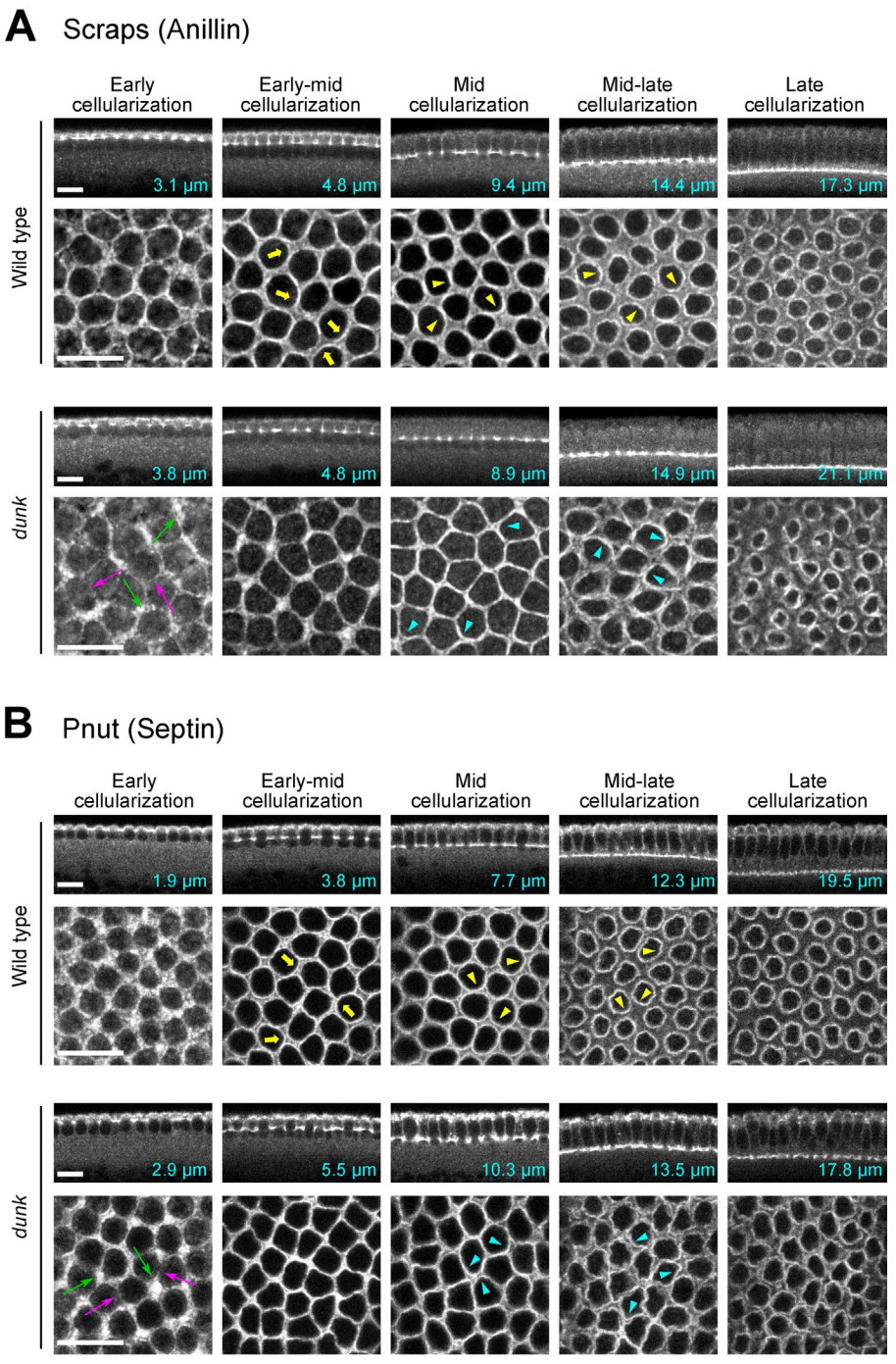

FIGURE 3: Dunk regulates the localization of anillin and the septin Pnut during cellularization. Anillin (A) and the septin Pnut (B) are mislocalized in *dunk*^{1} mutant embryos. Immunostaining showing the localization of Scraps (A) and septin Pnut (B) in cross-sections (top) and en face sections at the furrow canals (bottom). Anillin and septin show similar defects in *dunk*^{1} mutant embryos. During early cellularization, anillin, and septin are recruited to the furrow canals, but their spatial distribution at the furrow canals appears to be less homogeneous compared with the wild-type controls. The signal is often enriched at the vertices (green arrows) and depleted from the edges (magenta arrows). During early to midcellularization, anillin and septin in the control embryos become enriched at the nascent contractile rings (yellow arrows). In contrast, there is no clear sign of ring formation for anillin or septin in *dunk*^{1} mutant embryos at the similar stage. Although anillin and septin in the mutant embryos eventually form individual rings during mid- to late-cellularization, the rings are less circular and more irregular (cyan arrowheads) compared with those in the wild-type embryos (yellow arrowheads). Furrow depth is indicated in cyan. Note that the signal intensity of the en face view of the embryos at mid–late and late-cellularization was normalized based on the cytoplasmic signal. All scale bars:10 µm.

rings were often not well resolved (Figure 3A, cyan arrowheads). Finally, after the basal rings were formed in *dunk* mutant embryos, they were able to contract and became smaller over time (Figure 3A, "Late cellularization"). The apparent delay in the ring formation, the abnormal ring morphology, as well as the ability of the ring to contract is all analogous to the basal myosin phenotype in *dunk* mutant embryos (He *et al.*, 2016). The septin subunit Pnut, which depends on anillin to be recruited to the furrow canals during cellularization (Field et. al, 2005), showed similar localization defects as anillin in *dunk* mutant embryos (Figure 3B). Together, these results indicate that although Dunk is not crucial for the recruitment of anillin and septin to the cellularization front, it plays an important role in regulating their spatial organization across the basal array and facilitating their rearrangement into ring configurations.

Next, we sought to determine the earliest stage when the anillin mislocalization phenotype emerges in *dunk* mutant embryos. To this end, we performed live imaging of embryos expressing fluorescently-tagged anillin during the transition between the syncytial and cellularization stages. We were not able to use endogenously tagged anillin-mCherry for this purpose due to difficulties in recombining *anillin-mCherry* onto the *dunk* mutant chromosome. Instead, we used a previously described GFP-tagged anillin line (Silverman-Gavrila *et al.*, 2008). Of note, the expression of GFP-anillin was driven by UAS and maternal GAL4, which resulted in a substantial embryo-to-embryo variation in the expression level. To minimize the impact of this variation, we focused on comparisons between embryos with similar GFP-anillin intensity levels. To visualize anillin localization within each individual mitotic figure at the onset of cellularization, we generated maximum intensity projections for both the apical region (0–1.5 µm) and a slightly deeper region (3–4 µm below the surface) that covered the tip of pseudocleavage furrows (old furrows) from previous mitosis (Figure 4A). Anillin has been shown to localize to old furrows during syncytial divisions (Silverman-Gavrila *et al.*, 2008). Therefore, we used the anillin signal on the old furrows as a marker for outlining mitotic figures. In wild-type embryos, anillin-GFP first appeared as discrete puncta at the apical region ~ 1 or 2 min before the formation of cleavage furrows. These anillin puncta are distributed broadly over the apical cortex of each mitotic figure. Some puncta were away from the incipient cleavage furrow (Figure 4, B and D, white arrows; Figure 4C, white

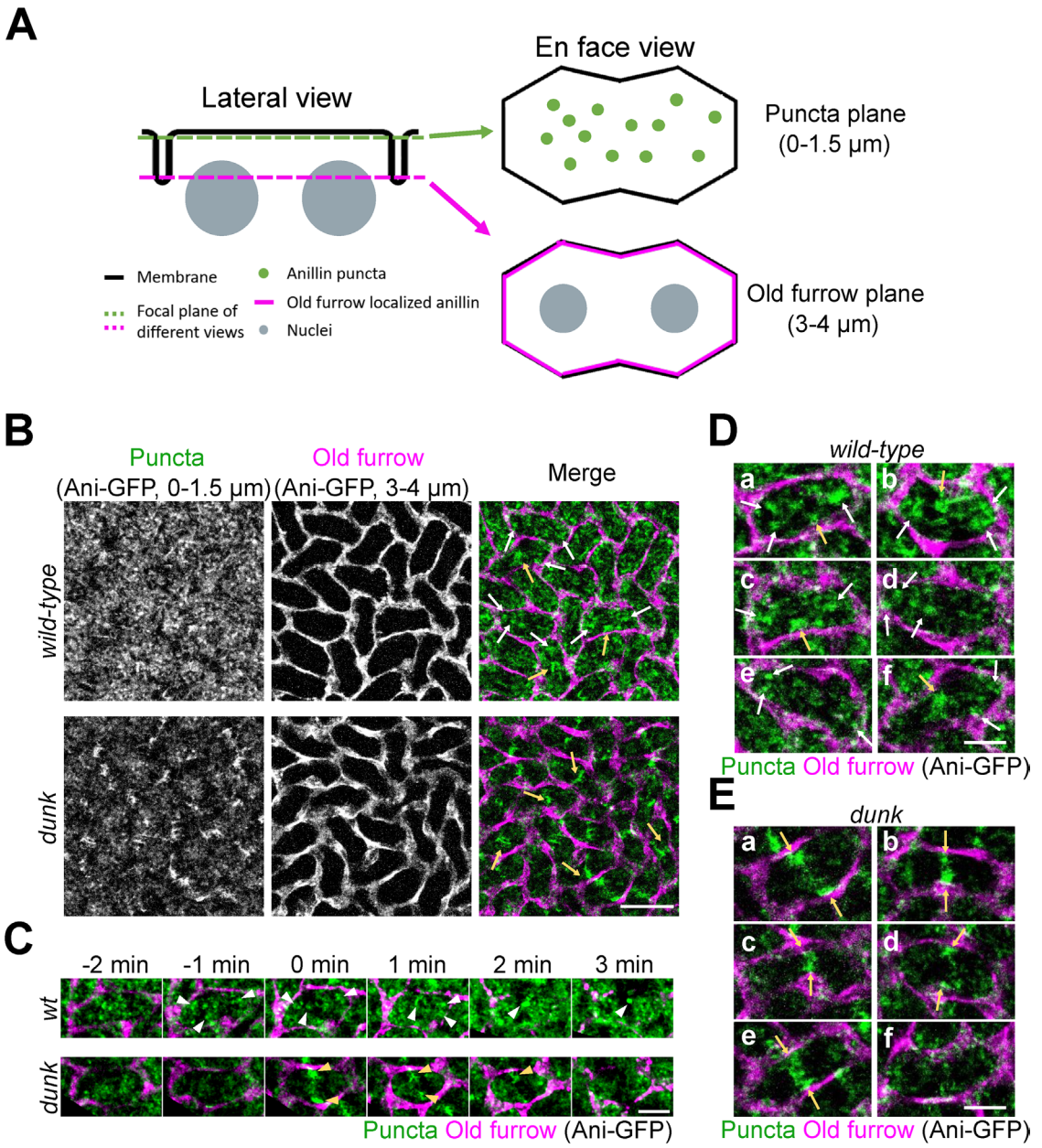

FIGURE 4: *dunk* mutant embryos show mislocalization of apical anillin puncta at the onset of cellularization. (A) Schematic representation of a single mitotic figure at the onset of cellularization, as seen from both lateral and en face perspectives. At the onset of cellularization, one mitotic figure refers to a pair of syncytial daughter nuclei resulting from the previous nuclear division cycle. Nascent cleavage furrows are expected to form at the midline of each mitotic figure. Residual pseudocleavage furrows, formed during the last syncytial division cycle, become the "old furrows" surrounding each syncytial mitotic figure. Anillin is both recruited to the old furrows (shown in magenta) and forms bright and distinct puncta (shown in green) at the apical cortex. (B) Projections of confocal sections display anillin-GFP at the apical (0–1.5 μm) and subapical (3–4 μm) zones of the cell membrane in wild-type and *dunk* mutant embryos at the onset of cellularization. The apical signals show anillin puncta, while subapical signals show anillin on old furrows. In the wild-type embryo, anillin puncta exhibit a relatively random localization at the cortex, covering nearly the entire surface of the mitotic figure. In the *dunk* mutant embryo, anillin puncta predominantly appear in the middle of the mitotic figure, where nascent furrows will form. White arrows: puncta appear away from the nascent furrow. Yellow arrows: puncta appear in the vicinity of the nascent furrow. Scale bar: 10 μm. (C) Anillin-GFP signal of one representative mitotic figure over time in wild-type and *dunk* mutant embryos. In the wild type, small anillin puncta (white arrowheads) appear randomly within the mitotic figure, merging into a larger and brighter punctum at the position of the nascent furrow at T = 2 min. This bright, large punctum moves basally as the membrane ingresses (T = 3 min). In the *dunk* mutant, anillin puncta appear at the nascent furrow starting at T = 0 (yellow arrowheads). These puncta also move basally as the membrane ingresses at T = 3 min. T = 0 represents the onset of cellularization. Scale bar: 5 μm. (D and E) Representative mitotic figures for wild-type embryos (D) and *dunk* mutant embryos (E) at T = 0 showing the initial appearance of anillin puncta. White arrows: puncta appear away from the nascent furrow. Yellow arrows: puncta appear in the vicinity of the nascent furrow. Scale bar: 5 μm.

arrowheads), while others were in the vicinity of the incipient furrow near the midline of the mitotic figure (Figure 4, B and D, yellow arrows). The number and size of anillin puncta within one mitotic figure were noticeably variable between different mitotic figures. As cellularization progressed, anillin puncta ultimately concentrated at the newly formed cleavage furrow, merging into larger puncta and moving basally as the membrane ingressed (Figure 4C, white arrowheads). In *dunk* mutants, we observed a striking difference in anillin localization at the onset of cellularization. ~18% of the mitotic figures in *dunk* mutant did not contain any obvious punctum structures (14 out of 79 mitotic figures in four embryos, e.g., Figure 4E, panel f). For the rest of the mitotic figures, Anillin puncta still formed apically in the absence of Dunk, however, fewer puncta were formed, and the location of the puncta was strongly biased towards the incipient furrow as they first appeared around the onset of cellularization (Figure 4, B and E, yellow arrows; Figure 4C, yellow arrowheads). While it remains uncertain about how the initial anillin puncta phenotype in *dunk* mutant embryos is linked to the anillin-mislocalization phenotype at the basal array, our observations suggest that the function of Dunk in regulating anillin can be traced back to the onset of cellularization and is required for the proper formation and localization of anillin puncta during the establishment of cleavage furrows.

The localization of Dunk at the cellularization front is not dependent on anillin

Next, we sought to determine whether anillin reciprocally regulates the localization of Dunk during early cellularization. To test this, we examined Dunk localization in *anillin*-maternal mutant embryos by immunofluorescence. We also examined the localization of Pnut as a control because its cortical localization depends on anillin (Field *et al.*, 2005). The *anillin*-maternal mutant embryos used in this study were derived from females that are trans-heterozygotes for two *anillin* mutant alleles (*anillin*$^{PQ/RS}$, hereafter "*anillin* mutant"; Schupbach and Wieschaus, 1989; Field *et al.*, 2005; Supplemental Figure S2). During early cellularization, Dunk and Pnut were evenly distributed across the basal hexagonal array in wild-type embryos (Figure 5). In *anillin* mutant embryos, Pnut signal was almost completely absent from the basal array, consistent with the previous study (Field *et al.*, 2005). In contrast, we found that Dunk was still recruited to the cellularization front and displayed normal spatial distribution in the absence of anillin (Figure 5). Interestingly, we frequently observed bright Dunk puncta at the basal cell–cell boundaries in *anillin* mutant embryos but not in wild-type embryos (Figure 5, red arrows). The nature of this structure as well as why it only appeared in *anillin* mutant embryos were unclear. We noticed that there was some embryo-to-embryo variation in the intensity of Dunk staining at the basal array, presumably due to inhomogeneity during immunostaining and/or sample mounting, but on average we did not observe an obvious difference between wild-type and *anillin* mutant embryos (Supplemental Figure S3). Of note, although the PQ and RS mutations are within the C-terminal domain of anillin (Field *et al.*, 2005), our yeast two-hybrid experiments demonstrated that both anillin^{PQ} and anillin^{RS} proteins interact with Dunk to a similar degree as wild-type anillin (Supplemental Figure S2A). Previous studies have shown that the localization of the mutant anillin^{PQ} and anillin^{RS} proteins at the cellularization front is significantly reduced (Field *et al.*, 2005). Thus, the observation that Dunk was still normally localized in *anillin* mutant embryos indicates that the localization of Dunk to the basal array does not depend on anillin. Taken together, the results of our localization studies suggest that Dunk functions upstream of anillin to regulate its localization at the cellularization front.

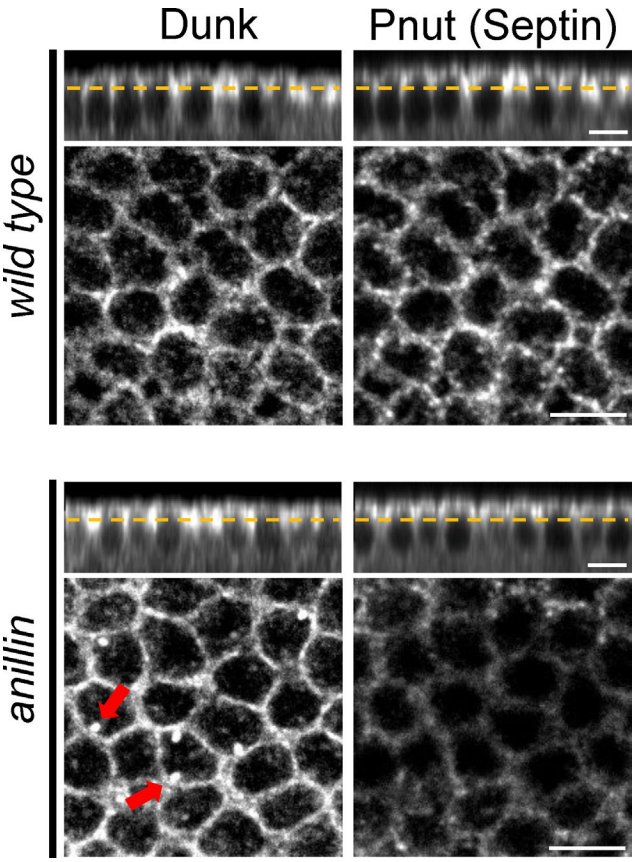

FIGURE 5: Dunk's cortical localization is not disrupted in *anillin* mutant. Wild-type or *anillin*$^{PQ/RS}$ mutant embryos were stained by Dunk or Pnut antibodies. Immunostaining showing localization of Dunk and septin (Pnut) in cross-sections (top) and en face sections at the furrow canals (bottom) during early cellularization. In *anillin* mutant embryos, Dunk remains uniformly distributed across the cellularization front and has an intensity level similar to that in wild-type embryos. In contrast, the recruitment of septin to the cellularization front is largely disrupted in the absence of anillin, showing only a faint signal. Yellow dashed line: cellularization front. Red arrows: Dunk puncta at the basal cell–cell boundaries in *anillin* mutant embryos but not in wild-type embryos. Scale bars: 10 μm.

Genetic interaction between *anillin* and *dunk*

The physical and functional links between Dunk and anillin prompted us to further examine potential genetic interactions between *dunk* and *anillin* mutant alleles. Previously identified *anillin* and *dunk* mutants were all characterized as recessive alleles. No obvious phenotypes have been reported for *anillin* or *dunk* heterozygous mutants (Field *et al.*, 2005; He *et al.*, 2016). If anillin and Dunk function in the same pathway regulating basal myosin network during cellularization, simultaneously reducing the amount of both proteins by double heterozygosity might impair the pathway to a degree that can result in detectable lesions. To test this, we generated *anillin*/*dunk* double-heterozygous mutants and asked whether it shows any synthetic phenotypes during cellularization. In the analysis described below, the *anillin* heterozygous (*ani*/+) refers to the maternal genotype, whereas the *dunk* heterozygous (*dunk*/+) refers to the zygotic genotype (*Methods*). In addition, all embryos contained maternally expressed myosin marker GFP-tagged Sqh (Spaghetti squash, myosin regulatory light chain, under the control of the *sqh* promotor; Royou *et al.*, 2002).

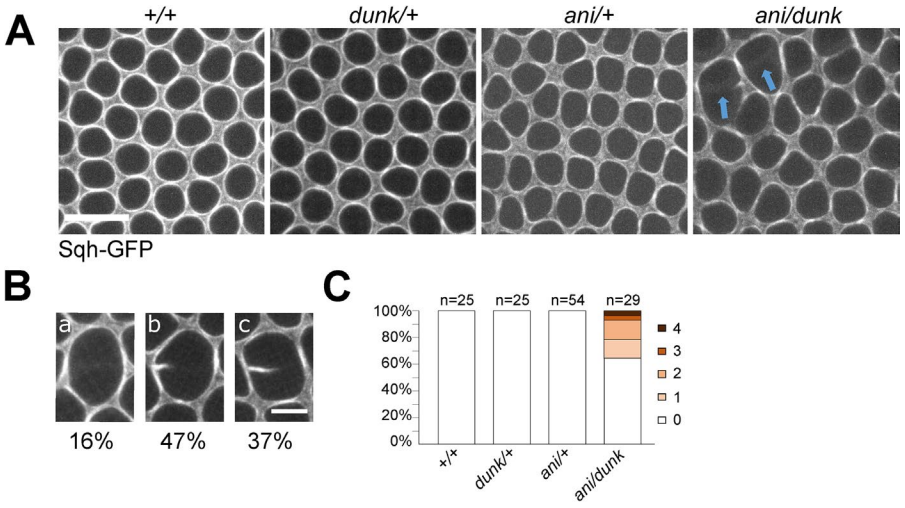

FIGURE 6: Genetic interaction between *dunk* and *anillin*. (A) Basal myosin organization in wild type (+/+), *dunk*-heterozygous mutants (*dunk*/+), *anillin*-heterozygous mutants (*ani*/+), and *anillin dunk* double-heterozygous mutants (*ani/dunk*). '*anillin*' here refers to the maternal genotype and '*dunk*' here refers to the zygotic genotype. Shown are representative images of basal myosin rings in mid to late-cellularization. The "broken-myosin-edge" phenotype, which refers to the loss of basal myosin signal from at least half of an edge between a pair of neighboring cells, was only observed in the double-heterozygous mutant embryos (blue arrows). Scale bar: 10 μm. (B) Enlarged view of different types of "broken-myosin-edge" phenotype observed in the double-heterozygous mutant embryos. a, b, and c show loss of myosin signal from the entire edge, 66.7–100% of the edge and 50–66.7% of the edge, respectively. The numbers below the images show the frequency of each type. Scale bar: 5 μm. (C) The fraction of embryos showing 1–4 broken-myosin-edges in the imaged region (~7% of the entire embryo surface). The "broken-myosin-edge" phenotype only exists in double-heterozygous mutant embryos. The numbers of embryos analyzed for each genotype are shown in the figure.

We first acquired snapshots of basal myosin in embryos at mid-cellularization when myosin rings have formed in wild-type embryos. We found that mutating one copy of *anillin* or *dunk* did not have a significant impact on basal myosin rings (Figure 6A). Interestingly, in about a third of the *anillin/dunk* double-heterozygous embryos (10 out of 29 embryos; the imaged region covered ~7% of the total embryo surface), when basal myosin first reorganized into individual rings, we observed "broken" myosin edges between one or more pairs of neighboring cells (Figure 6A, arrows). In some cases, the entire edge was missing (Figure 6B, "a"). In other cases, myosin was missing from a part of the edge (Figure 6B, "b" and "c": missing from 66.7–100% and 50–66.7% of the edge, respectively). We did not observe obvious bias in the location of the breaks within the imaged region. This "broken-myosin-edge" phenotype was only observed in the double heterozygous mutant, but not in the wild type or either of the single heterozygous mutants (Figure 6C). Therefore, simultaneously reducing the amount of Dunk and anillin to the level of heterozygous mutant generates a synthetic effect on basal myosin organization during cellularization.

We next wondered whether the synthetic effect on myosin organization can be detected at an earlier stage before the basal myosin network reorganized into discrete contractile rings. To this end, we acquired movies that covered early cellularization stages (T = 0–10 min). In both single and double heterozygous-mutant embryos, the basal myosin array formed at about the same time as in wild-type embryos, but subtle differences in the arrangement of basal myosin array could be detected between genotypes (Supplemental Figure S4A). While the localization of myosin at the basal array in *dunk*/+ embryos was nearly identical to that in wild-type embryos, the localization of myosin is more heterogeneous in *ani*/+ and *anillin/dunk* embryos, with a biased enrichment at the vertices and depletion from the edges (Supplemental Figure S4A, green and magenta arrows, respectively). The biased distribution of myosin was more prominent in *anillin/dunk* embryos than in *anillin*/+ embryos, which we confirmed by quantifying the vertex/edge ratio of myosin intensity at T = 10 min (Supplemental Figure S4, A and B). Together, the observed additive effects of *ani*/+ and *dunk*/+ on basal myosin organization support the notion that Dunk and anillin function together to regulate basal myosin organization during cellularization.

dunk bnk double mutants show similar myosin phenotype during cellularization as *anillin bnk* double mutants

To further test the functional link between Dunk and anillin, we examined their genetic interactions with the cellularization-specific gene *bnk*. During cellularization, *bnk* regulates the reorganization of basal myosin network into individual contractile myosin rings (Schejter and Wieschaus, 1993). In *bnk* mutant embryos, the basal actomyosin array reorganizes into contractile rings prematurely and displays hyper-contractility (Figure 7, A, A′, A″, B, B′, and B″; Schejter and Wieschaus, 1993). A previous study shows that when *anillin* and *bnk* are both mutated, the phenotypes of every single mutant are coexpressed: in the absence of anillin, the structural organization of basal myosin is impaired, whereas a further increase in actomyosin contractility caused by lack of Bnk results in rupturing of the basal network in cellularization (Thomas and Wieschaus, 2004). We reasoned that if Dunk and anillin function in the same pathway in early cellularization, combining mutations in *dunk* and *bnk* would generate a similar phenotype. Indeed, we found that unlike the *dunk* mutant embryos where the basal array appeared intact without obvious ruptures (comparing Figure 7, A, A′, A″, C, C′, and C″), the basal network in *bnk dunk* mutant embryos was severely disrupted, yielding large holes at the furrow canals that encloses multiple nuclei (Figure 7 D, D′, and D″, magenta arrows). These holes were usually circular, suggesting that the ruptured basal array was still under tension. In addition, at regions where rupture did not occur, basal myosin displayed hyper-constricted phenotype as in *bnk* mutant embryos (comparing Figure 7, B′ with D′, cyan arrowheads). These observations demonstrate that similar to *bnk* and *anillin*, the *bnk* and *dunk* phenotypes are also coexpressed in the double-mutant embryos. The *bnk dunk* double-mutant phenotype is in sharp contrast to that of the *bnk src64* double mutant, in which the *bnk* phenotype is suppressed by the removal of Src64, a positive regulator of actomyosin contractility (Thomas and Wieschaus, 2004). These results are consistent with the notion that Dunk does not function to activate myosin contractility, but rather functions to maintain the structural integrity of the basal actomyosin structures (He *et al*., 2016). The similarity in the basal myosin phenotype between *dunk bnk* and *anillin bnk* double-mutants provides further support to the model where Dunk and anillin function in the same pathway to regulate basal myosin in cellularization.

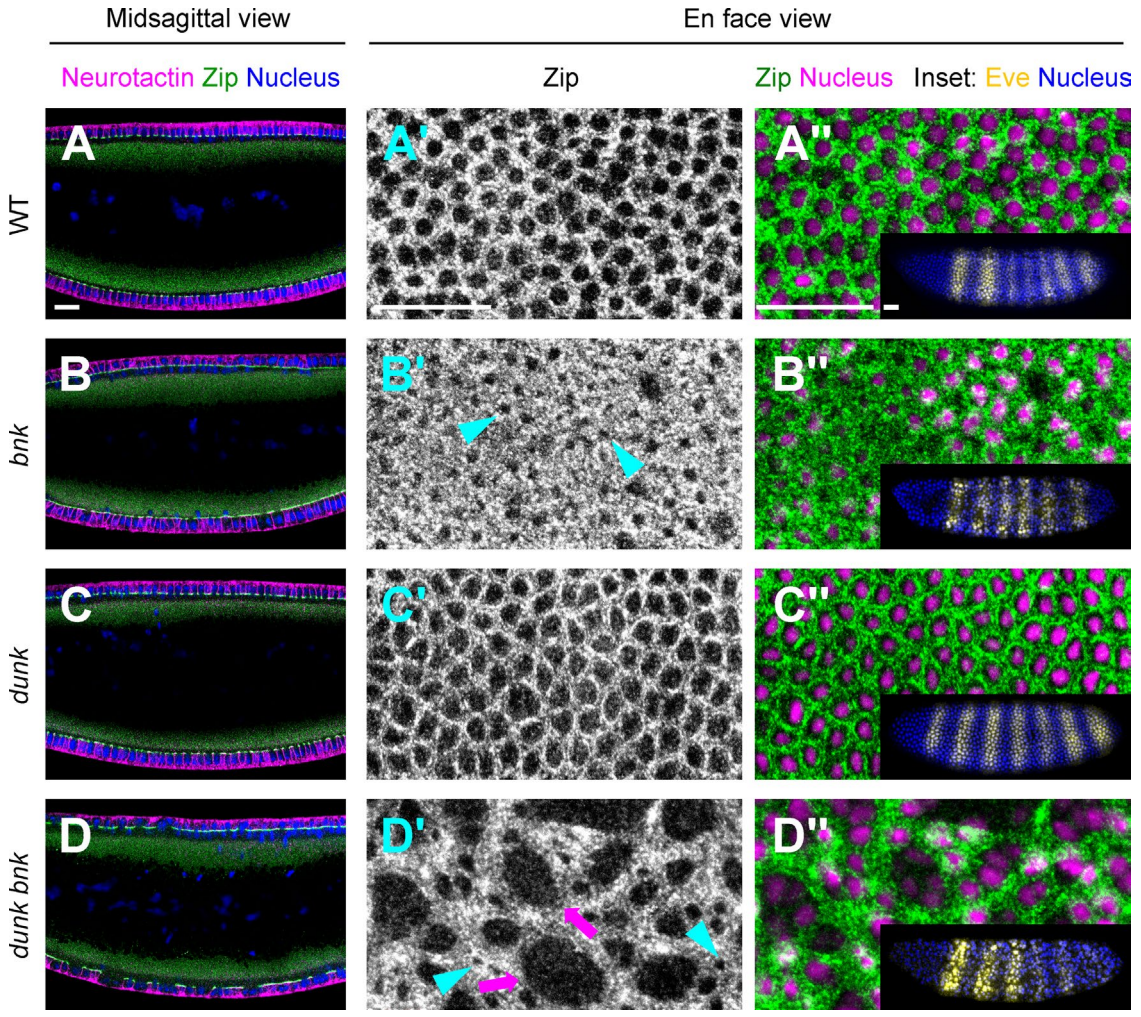

FIGURE 7: Increasing basal actomyosin contractility exacerbates the myosin phenotype in *dunk*^{1} mutant embryos. (A, A′, and A″) wild-type (WT) embryo. (B, B′, and B″) *bnk* mutant embryo. (C, C′, and C″) *dunk*^{1} mutant embryo. (D, D′, and D″) *bnk dunk*^{1} double-mutant embryos stained with Neurotactin, Zipper, DAPI, and Eve. A–D: cross-sections of embryos showing staining for membrane (Neurotactin), Zipper, and nucleus. A′–D′ and A″–D″: projections of confocal sections showing the en face view of the furrow canals as marked by Zipper. The phenotypes of *dunk* and *bnk* are coexpressed. The disruption of *dunk* in *bnk* mutant leads to a combined phenotype of premature ring contractions (*bnk*, cyan arrowheads) and reduced integrity of the basal actomyosin network (*dunk*), causing the tearing of the network (magenta arrows). Inset in A″–D″: immunostaining of Eve, which was used to identify *bnk* mutant embryos (*Methods*). *Df(3R)*$^{tll\text{-}e}$, the deficiency used to generate *bnk* mutant embryos, contains a deletion that covers both *bnk* and the terminal gap gene *tll* (Schejter and Wieschaus, 1993). Tll regulates the expression of pair-rule genes in a stereotyped manner (Frasch and Levine, 1987). *tll* mutant embryos show six Eve strips instead of seven as in the wild-type embryos. All scale bars: 20 μm.

Anillin colocalizes with myosin and shows similar cortical dynamics as myosin in early cellularization

Our results so far support a model where Dunk functions upstream of anillin in regulating basal myosin array during early cellularization. While the role of anillin in regulating actomyosin ring during cytokinesis has been well demonstrated in various species and cell types, including cellularization (Field *et al.*, 2005; Piekny and Glotzer, 2008; Piekny and Maddox, 2010), the function of anillin before the formation of cytokinetic rings is less explored. We therefore sought to investigate whether anillin has an early function in cellularization to regulate myosin recruitment and organization, starting by asking whether anillin colocalizes with myosin during early cellularization.

To test colocalization between anillin and myosin, we performed live-imaging analysis with embryos coexpressing GFP-anillin (under the control of UAS-Gal4; Silverman-Gavrila *et al.*, 2008) and mCherry-tagged Sqh (under the control of the *sqh* promotor; Martin *et al.*, 2009). We found that during mid–late cellularization, anillin and myosin colocalized with each other at the basal contractile rings (Figure 8; T = 30–40 min), consistent with previous reports (Field *et al.*, 2005). In addition, anillin and myosin also showed extensive colocalization at the basal myosin array before the formation of myosin rings (Figure 8; T = 5–25 min). As the basal myosin array started to form a few minutes into cellularization, the edges of the array were wide and fuzzy, and the myosin signal appeared to be patchy (Figure 8; Supplemental Figure S5, T = 5 min). At this early stage, anillin was also enriched in the basal network and partially colocalized with myosin (Figure 8; Supplemental Figure S5, T = 5 min). As the edges of the basal array tightened over time, the colocalization between anillin and myosin became more prominent, and the two proteins eventually nearly completely overlapped at the cellularization front (Figure 8, T = 10–25 min; Supplemental Figure S5, T = 15 and 25 min). Immunostaining of anillin and zipper, the myosin heavy

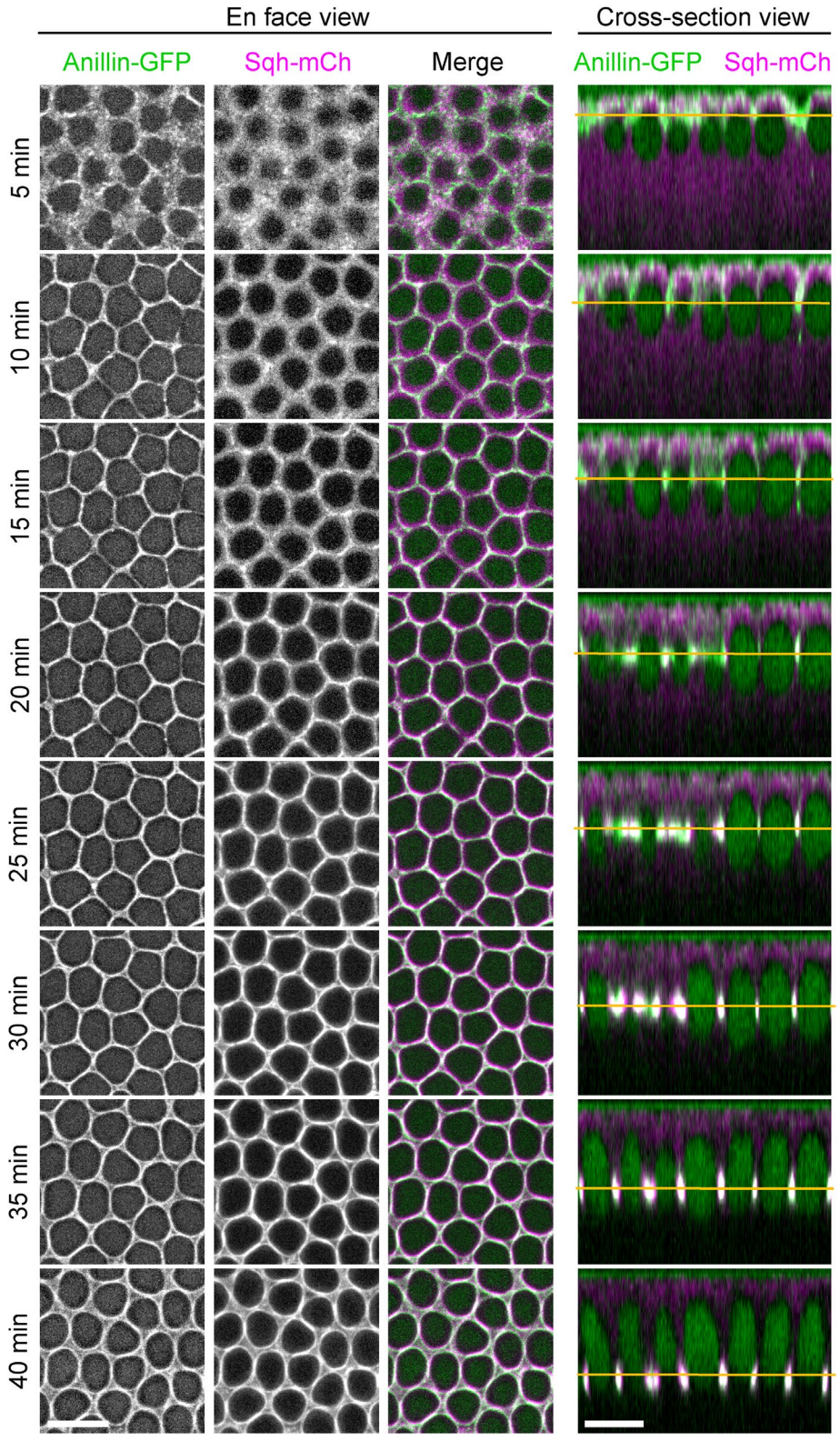

FIGURE 8: Localization of anillin and myosin during early and midcellularization. Live imaging of wild-type embryos expressing anillin-GFP and Sqh-mCherry. Left panels: en face view, maximum projections of 2–3 µm confocal sections covering the furrow canals; right panels: cross-sectional view generated by reslicing of confocal z-stacks. The intensities of the en face views have been individually adjusted to better demonstrate the colocalization of the two proteins. Anillin and myosin partially colocalize at the furrow canals during early cellularization (T = 5 min). The colocalization becomes more extensive after T = 10 min, and the two proteins remain colocalized throughout mid to late-cellularization as the basal array reorganizes into individual rings. Yellow lines: cellularization front. Scale bars: 10 µm.

chain, lead to similar observations (Supplemental Figure S6).

Interestingly, live-imaging analysis showed that the colocalization between myosin and anillin could be traced all the way back to the onset of cellularization (Figure 9, A and B, T = 0 s, defined by the formation of daughter nuclei after the last syncytial nuclear division). At ~ T = –2 min, myosin and anillin appeared and colocalized as punctum-like structures at the apical domain, with a moderate enrichment near nascent cleavage furrows (Figure 9B, colocalization: red arrow). Immediately after their first appearance, the puncta that were away from the nascent furrow moved towards the furrow (Figure 9C, orange arrows), whereas those first appeared in the vicinity of the nascent furrow remained where they were (Figure 9C, cyan arrows). Both behaviors contributed to the enrichment of myosin and anillin at the nascent furrows. Within an individual punctum, anillin, and myosin appeared around the same time and remained colocalized throughout the cortical movement (Figure 9C). The movement of myosin puncta towards the nascent furrow is consistent with the previous observation (He *et al.*, 2016), and we further extended this observation to anillin by demonstrating the coexistence of myosin and anillin in the puncta. Taken together, our results demonstrate an extensive colocalization between anillin and myosin at the cellularization front both before and after the formation of basal myosin rings.

Anillin regulates myosin localization during early cellularization

Next, we examined whether anillin regulates the formation and/or maintenance of the basal myosin array. To test this possibility, we imaged wild-type and *anillin* mutant embryos expressing GFP-tagged Sqh. We first focused on the localization of myosin at the cellularization front after the initial recruitment of myosin to the nascent furrows (Figure 10A). Compared to wild-type embryos, the spatial distribution of basal myosin was less uniform in *anillin* mutant embryos during the first 20 min of cellularization (Figure 10A). Specifically, the myosin signal was aberrantly enriched at the vertices and largely depleted from the edges (Figure 10A, 5–15 min, green and magenta arrows, respectively). As more myosin was recruited to the basal array over time, this "fragmented" basal myosin array phenotype became less prominent (Figure 10A, 20–30 min). To further quantify the "fragmented" basal myosin phenotype, we segmented the basal array and measured the myosin

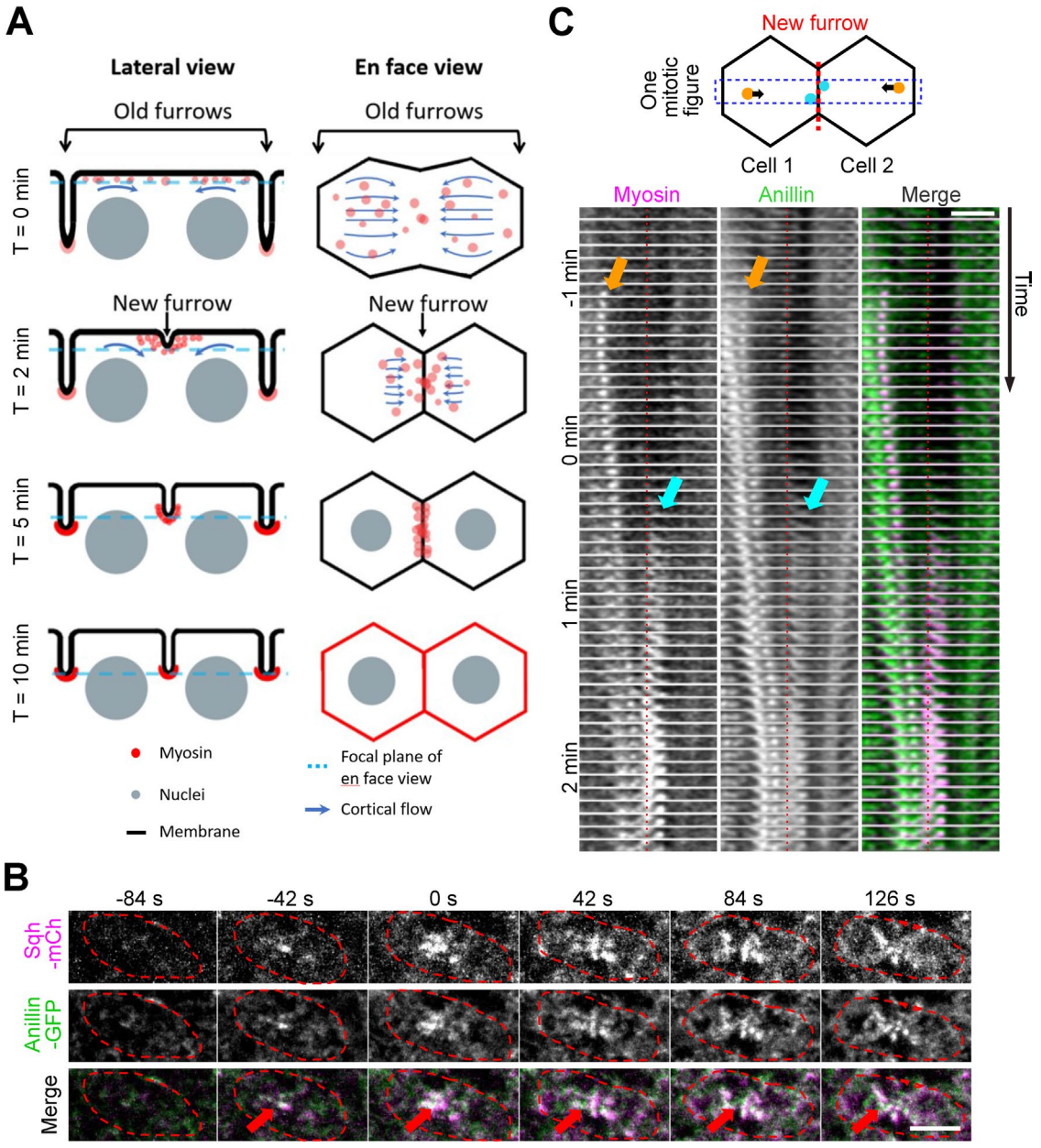

FIGURE 9: Anillin colocalizes and comoves with cortical myosin puncta at the onset of cellularization. (A) Schematic representation of a single mitotic figure during early cellularization, as seen from both lateral and en face perspectives. A cortical flow initiates around T = 0 min, driving punctum-like myosin structures to the "new furrows" located between daughter nuclei. As a result, myosin is concentrated at the nascent furrows and moves to the basal region as new furrows invaginate (T = 0–10 min). This cortical flow at the onset of cellularization is essential for myosin recruitment to the new furrows during the first 10 min of cellularization, resulting in myosin forming an interconnected hexagonal basal array at the cellularization front. During this period, the old furrows gradually retract toward the embryo's surface (~ 5 μm in length at T = 0 min and ~ 3 μm at T = 10 min), while new furrows continue to ingress. Once the new furrows and the old furrows attain the same length (~ 3 μm around T = 5–10 min), they extend synchronously and gradually increase in length over time. (B) Live imaging of wild-type embryos expressing anillin-GFP and Sqh-mCherry. Maximum projections of the apical z-slices (0–3 μm) of an embryo around the onset of cellularization (T = 0 s). Red arrows indicate the colocalization of anillin and myosin at the new furrow. Red dashed lines: the outline of the previous mitotic figure. Scale bar: 5 μm. (C) Top: a schema showing the apical anillin–myosin puncta in one mitotic figure. Some puncta (orange) first appear away from the nascent furrow (red dashed line) and move towards the new furrow (black arrows), whereas other puncta (cyan) first appeared at the nascent furrow. Blue box marks the region where the montage is generated. Bottom: montage showing the cortical flow of anillin and myosin puncta towards the newly formed cleavage furrow at the beginning of cellularization. Orange and cyan arrows indicate puncta corresponding to the orange and cyan puncta in the schematics, respectively. Red dashed lines mark the position of the nascent cleavage furrow. Scale bar: 5 μm. Time scale: 4.2 s per frame.

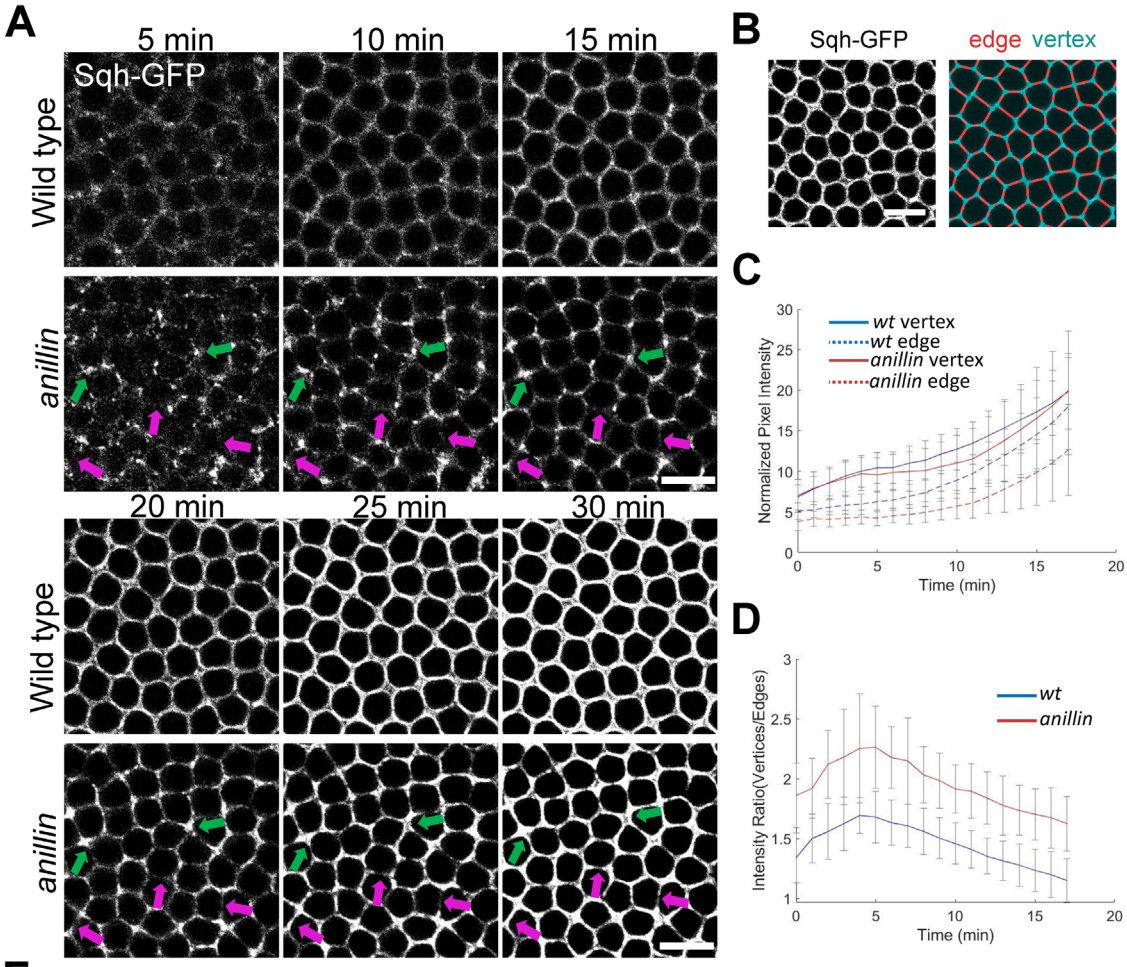

E

Time (minute)	0	1	2	3	4	5	6	7	8	9	10	11	12	13	14	15	16	17
p-values (vertex)	0.81	0.90	0.96	0.73	0.71	0.31	0.50	0.30	0.25	0.19	0.19	0.16	0.25	0.38	0.54	0.72	0.88	0.95
p-values (edge)	7.6E-03	1.2E-02	9.9E-04	1.1E-03	3.0E-03	4.5E-04	6.2E-04	8.6E-04	1.2E-03	5.9E-04	9.4E-04	6.0E-04	1.0E-03	4.4E-03	1.0E-02	1.7E-02	2.6E-02	3.9E-02
p-values (ratio)	4.0E-05	2.6E-04	3.7E-05	6.0E-04	1.3E-03	9.6E-05	1.0E-05	2.7E-04	3.3E-05	1.4E-05	7.6E-06	7.4E-06	4.1E-06	3.6E-05	1.3E-05	1.2E-05	4.8E-05	1.8E-05

FIGURE 10: *anillin* mutant embryos show abnormal basal myosin localization during early cellularization. Live imaging of wild-type and *anillin* mutant embryos expressing Sqh-GFP. (A) Maximum projections of confocal sections showing Sqh-GFP at the furrow canals in wild-type and *anillin*-maternal mutant embryos during the first 30 min of cellularization. Basal myosin distribution is abnormal in *anillin* mutant embryos. Specifically, during the first 20 min, myosin appears to be depleted from the edges (magenta arrows) and accumulated at some vertices (green arrows), closely resembling the previously reported myosin phenotypes in *dunk* mutant embryos (He *et al.*, 2016). Scale bar: 10 μm. (B) Schematic diagram showing quantification of myosin intensity at vertices (cyan) and edges (red). Scale bar: 10 μm. (C) Quantification of vertex- and edge-myosin intensities at the furrow canals in wild-type (blue) and *anillin* (red) mutant embryos. (D) The ratio between vertex- and edge-myosin intensities. Wild type, $n = 11$ embryos; *anillin*, $n = 12$ embryos. Error bars: SD (E) Statistical comparison between wild-type and *anillin* mutant embryos for the mean intensity at the vertices, the mean intensity at the edges, and the vertex/edge-mean intensity ratios. Two-tailed unpaired student's *t* test was used. Red indicates statistically significant ($p < 0.05$). Black indicates no significant difference ($p > 0.05$).

intensities at the vertices and edges, as previously described (Figure 10B; *Methods*; He *et al.*, 2016). The average myosin intensity at the vertices is comparable between wild-type and *anillin* mutant embryos; however, there was less myosin at the edges in *anillin* mutant embryos compared with the wild type (Figure 10, C and E). As a result, the vertex/edge ratio of myosin intensity is higher in the *anillin* mutant embryos than that in the wild-type embryos (Figure 10, D and E). The defects in the spatial organization of basal myosin array, in particular the biased localization of myosin at the vertices and depletion of myosin from the vertices, closely resembles the reported myosin phenotype in *dunk* mutant embryos (He *et al.*, 2016). This similarity is consistent with the notion that Dunk and anillin function in the same pathway to regulate cortical myosin organization during early cellularization.

To understand how basal myosin phenotype develops in *anillin* mutant embryos, we examined GFP-tagged Sqh at the transition between the syncytial and cellularization stages. We focused on the apical and subapical zones of the cell membrane from the time when myosin puncta first appeared until they moved away from most parts of the apical region. As previously described (He *et al.*, 2016), in wild-type embryos, myosin first appeared at the apical domain of each mitotic figure when the nuclei started to form (T = –1 min), which was 1 or 2 min before the formation of the new furrow between the daughter nuclei (T = 0 min; Figure 11A). Meanwhile,

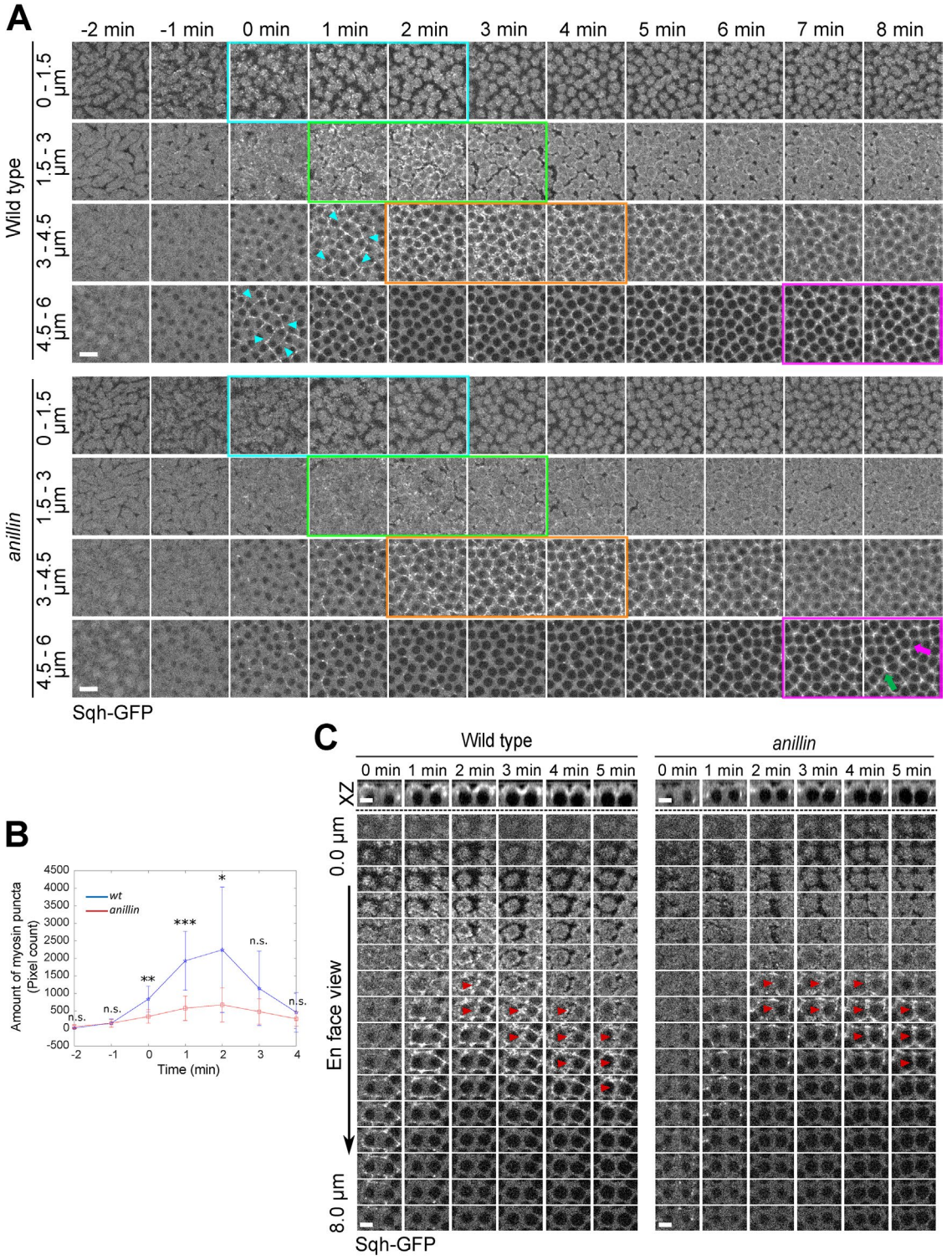

FIGURE 11: *anillin* mutant embryos show a reduced amount of apical myosin puncta which are less stable at the new furrow. (A) Projections of confocal sections showing Sqh-GFP at the apical and subapical zones of the cell membrane (0–1.5 µm, 1.5–3 µm, 3–4.5 µm, and 4.5–6 µm) in wild-type and *anillin* mutant embryos over time. In wild-type embryos, myosin puncta first appear at the apical cortex (cyan box) and the tip of retracting pseudocleavage furrows (cyan arrowheads) around the onset of cellularization. The apical puncta rapidly disappear from the apical surface as the furrows invaginate (green box). At T = 2–4 min, as myosin puncta have mostly disappeared from the 0–3 µm zone, myosin puncta become predominantly enriched at the 3–4.5-µm zone and uniformly decorate the leading edge of both old and new furrows (orange box). In *anillin* mutant embryos, myosin puncta at the 0–3-µm region were greatly diminished compared with the wild type, although the number of puncta showed a similar increase–decrease trend as the wild type (cyan and green boxes). At T = 2 min, myosin started to be recruited to the cellularization front in *anillin* mutant at the 3–4.5-µm zone and was more or less uniformly distributed at the leading edge at this point (orange box).

myosin appeared at the base of the remnant pseudocleavage furrows (the old furrows, Figure 11A, cyan arrowheads), which was retracting until ~ T = 2 min when the new furrow reached the similar depth as the old furrows (Figure 11A, orange box). The apical myosin puncta were initially quite sparse (T = −1 min) but the number increased rapidly and reached the peak at T = 1–2 min (Figure 11, A, cyan box, and B). The puncta then quickly disappeared from the apical surface as the furrows invaginate. At T = 0 min, myosin puncta also appeared at the 1.5–3-μm zone and followed the same increase–decrease trend as the apical myosin puncta, but with a 1-min lag (Figure 11A, green box). At T = 3–4 min, as myosin puncta have mostly disappeared from the 0–3-μm zone, myosin puncta became predominantly enriched at the 3–4.5-μm zone and uniformly decorated the leading edge of both old and new furrows (Figure 11A, orange box). In the next few minutes, the edges of the basal myosin array tightened as the furrows continued to invaginate (Figure 11A, magenta box).

In *anillin* mutant embryos, we observed two major differences from the wild-type embryos. First, myosin puncta at the 0–3-μm region were greatly diminished compared with the wild type, although the number of puncta showed a similar increase–decrease trend as in the wild type (Figure 11, A, cyan and green boxes, and B). This result indicates that anillin facilitates the formation of apical myosin puncta at the onset of cellularization. Second, basal myosin appeared to be less stable in *anillin* mutant embryos compared with the wild-type embryos. At ~ T = 2 min, myosin started to be recruited to the cellularization front at the 3–4.5-μm zone in *anillin* mutant embryos (Figure 11A, orange box). Although the number of myosin puncta recruited to the leading edge appeared to be slightly fewer compared with the control embryos, these puncta were more or less uniformly distributed at the cellularization front when they first appeared. Examination of individual mitotic figures also shows that myosin was recruited to the base of both old and new furrows (Figure 11C, red arrowheads indicate the new furrow). However, in the following several minutes, as the furrows continued to ingress (i.e., basal myosin moved deeper into the embryo), the myosin signal became progressively diminished at the edges and concentrated at the vertices, resulting in the fragmented basal myosin array phenotype (Figure 11A, magenta box and magenta and green arrows show depletion and enrichment of the myosin signal, respectively). These results suggest that anillin has two roles during the flow phase of myosin recruitment. First, anillin is required for the formation of apical myosin puncta at the onset of cellularization. The flow of these myosin puncta to the nascent furrows contributes to initial myosin recruitment to the cellularization front. Second, anillin facilitates the retention of myosin at the base of the ingressing furrows, which is important for the formation of an interconnected basal myosin array and the subsequent assembly of myosin rings.

Of note, while the basal myosin phenotype in *anillin* mutants during early cellularization resembles that in *dunk* mutants, the myosin phenotype during late cellularization is different between the two genotypes. In *dunk* mutant embryos, basal myosin rings still form and contract to mediate basal closure of the nascent cells (He *et al.*, 2016). Although the myosin rings in the *dunk* mutant embryos appear less circular compared with those in the wild-type embryos (Supplemental Figure S7A, red arrows), there is no obvious difference in the rate of ring closure between the two genotypes (Supplemental Figure S7B). In contrast, the proper myosin ring formation and subsequent ring closure are both defective in *anillin* mutant embryos (Field et al, 2005). In addition to the rate of ring closure, the rate of cleavage furrow ingression is also differently impacted in *dunk* and *anillin* mutants. Previous studies have shown that the rate of furrow ingression is moderately impaired in *anillin* mutant embryos (Field *et al.*, 2005), which we confirmed in our own experiments examining furrow ingression in maternal *anillin*$^{PQ/RS}$ mutant embryos (Supplemental Figure S2, B and C). In contrast, our previous study has shown that *dunk* mutant embryos exhibit no obvious defects in the rate of furrow ingression during cellularization (He *et al.*, 2016). Together, these observations suggest that in addition to the function of regulating the basal myosin network downstream of Dunk during early cellularization, anillin also facilitates furrow ingression and basal myosin ring assembly and constriction, which are independent of Dunk's activity.

DISCUSSION

The proper recruitment of myosin to the cleavage furrow is a critical step in animal cytokinesis (Normand and King, 2010; Piekny and Maddox, 2010; Green *et al.*, 2012). *Drosophila* cellularization offers an advantageous system to study the mechanism of myosin recruitment and organization during cytokinesis, as several thousands of cleavage furrows form synchronously on the embryo surface, accompanied by rapid, simultaneous recruitment of myosin to the entire array of nascent cleavage furrows (Royou *et al.*, 2004; He *et al.*, 2016). Previous identification of *dunk*, a cellularization-specific gene that regulates the initial recruitment of myosin to the basal array, provides a useful molecular handle to investigate the mechanism of this process (He *et al.*, 2016). In this study, we identified the well-conserved cytokinetic scaffolding protein anillin as a binding partner of Dunk. Further domain analysis demonstrates that Dunk binds to the C-terminal region of anillin, and this binding requires the PH domain and is greatly enhanced by the presence of the AH domain and the ~ 200 a.a. sequence more N-terminal to the AH domain. We further present evidence that Dunk functions upstream of anillin to regulate basal myosin during early cellularization. First, we show that Dunk and anillin colocalize with each other at the cellularization front. Loss of Dunk results in the mislocalization of anillin and septin within the basal array and causes defects in the formation of basal anillin and septin rings. On the other hand, Dunk's localization to the basal array does not require anillin. Second, we show that *dunk* and *anillin* have genetic interactions. Mutant embryos that are heterozygous for

In the following several minutes, as the furrow continued to ingress, the myosin signal became progressively diminished at the edges (magenta arrow) and concentrated at the vertices (green arrow), resulting in the fragmented basal array phenotype (magenta boxes). Scale bar: 10 μm. (B) Quantification of myosin puncta at the apical cortex (0–2.5 μm) in wild-type (WT) and *anillin* mutant embryos over time. The quantification measures the number of pixels of all myosin intensity in the view after segmenting the puncta by thresholding (*Methods*). Error bars: SD A two-tailed unpaired student's *t* test was used for statistical comparison. Wild type, $n = 7$ embryos; *anillin*, $n = 10$ embryos. *, $p < 0.05$; **, $p < 0.01$; ***, $p < 0.001$; not significant, $p > 0.05$. (C) Examination of individual mitotic figures over time. Top panel: cross-sectional view of one mitotic figure. Bottom panel: the montage of myosin signal over time at different depths. In *anillin* mutant embryos, when myosin was recruited to the cellularization front at T = 2 min, it decorated the base of both old and new furrows (Red arrowheads indicate the position of the new furrow). Scale bar: 5 μm.

both *dunk* and *anillin* loss of function mutations have synthetic defects in basal myosin organization. In addition, *dunk* and *anillin* mutants show identical synthetic phenotypes when combined with *bnk* mutant that causes enhanced contractility of the basal actomyosin network. Finally, we show that anillin colocalizes with myosin at the cellularization front during the formation of cleavage furrows and regulates the initial recruitment of myosin and its localization at the basal array. This previously unappreciated function of anillin in regulating basal myosin array is similar to the reported function of Dunk (He *et al.*, 2016). Together, these results led us to propose that Dunk regulates myosin at the furrow canals by interacting with anillin and controlling anillin's localization and/or activity.

Although the function of anillin in regulating actomyosin ring during cytokinesis has been well demonstrated (Field *et al.*, 2005; Piekny and Glotzer, 2008; Piekny and Maddox, 2010), the understanding of its function before the ring formation remains limited. Our quantitative analysis of Sqh-GFP in *anillin* mutants shows that in the absence of functional anillin, less myosin was recruited to the apical cortex at the onset of cellularization. Furthermore, the stability of myosin recruited to the basal array was reduced, causing the aberrant spatial-distribution of myosin across the leading edge of the furrows. These observations indicate that in addition to the well-conserved role of anillin in regulating myosin ring assembly, anillin also regulates myosin recruitment and maintenance at the cellularization front before myosin ring formation. Most interestingly, we found that at the onset of cellularization when myosin was first recruited to the apical cell cortex as punctum-like structures, anillin colocalizes with myosin puncta and comove with myosin towards the nascent-cleavage furrow. Furthermore, we found that the initial formation of cortical puncta of anillin is regulated by Dunk. In *dunk* mutant embryos, anillin puncta exhibited a more pronounced "midline localization" in most mitotic figures, in contrast to the broad distribution at the apical cortex of each mitotic figure in wild-type embryos. These observations define the earliest stage in cellularization when Dunk regulates anillin. An important future question is how the defects in myosin and anillin puncta assembly at the onset of cellularization contribute to the later phenotype of aberrant myosin and anillin distribution at the basal array. In a broader context, the cortical flow of myosin towards the prospective cleavage furrow has been observed in various cytokinesis contexts (DeBiasio *et al.*, 1996; Yumura *et al.*, 2008; Uehara *et al.*, 2010; He *et al.*, 2016). It would be of interest to investigate whether anillin is also involved in cortical myosin flow during other cytokinesis processes and whether other cytokinetic proteins are cotransported with the flow.

It remains to be addressed how anillin promotes myosin recruitment and cortical retention during early cellularization. Anillin may help activate myosin through its interaction with RhoA. A recent study suggests that anillin promotes RhoA activation by increasing the membrane residence time of RhoA (Budnar *et al.*, 2019). It would be of interest to investigate whether the function of anillin and Dunk is required for the proper activation of RhoA at the onset of cellularization. Alternatively, anillin may facilitate the cortical localization of myosin by serving as cortical binding sites for myosin through direct interactions. Interestingly, previous study has shown that although Dunk promotes the cortical retention of myosin during early cellularization, loss of Dunk does not affect the rate of myosin turnover at the cell cortex (He *et al.*, 2016). This leads to the hypothesis that Dunk may regulate myosin retention by controlling the available myosin-binding sites at the cell cortex, rather than controlling the dynamic interaction of myosin with the binding sites per se. Thus, the potential role of anillin serving as a cortical myosin-binding site during early cellularization is an intriguing avenue of future direction.

Notably, the defect in basal myosin accumulation seen in the *anillin* and *dunk* mutant embryos became less prominent after the first 20–25 min of cellularization (Field *et al.*, 2005; He *et al.*, 2016), suggesting that certain anillin- and Dunk-independent mechanisms for myosin activation/recruitment (e.g. Slam-dependent direct recruitment of myosin, He *et al.*, 2016) is in charge after the initial phase of cellularization. In addition, despite the similarity of the myosin phenotype in *dunk* and *anillin* mutant embryos during early cellularization, the *anillin* mutant, but not the *dunk* mutant, shows disrupted rearrangement of basal myosin into individual rings during midcellularization (Field *et al.*, 2005; He *et al.*, 2016). Therefore, while the early function of anillin in regulating myosin enrichment at the furrow canals is shared with Dunk, the late function of anillin in regulating myosin ring formation is independent of Dunk. These unique, temporally separable mechanisms for myosin recruitment and rearrangement during cellularization (He *et al.*, 2016; Xue and Sokac, 2016) make it an attractive system to reveal the stage-specific function and regulation of anillin during cytokinesis.

Like other cellularization-specific proteins, Dunk is not conserved in other model organisms. Sequence homologues of Dunk are only found in dipterans. This leads to the interesting question of why Dunk is required for regulating anillin in cellularization but not in conventional cytokinesis, including post-cellularization cytokinesis in flies. Despite all the similarities, cellularization is different from typical cytokinesis in a number of ways. One important difference is the cell cycle stage when the cleavage furrows are formed. Cellularization happens during the interphase of the cell cycle (Foe and Alberts, 1983), while typical cytokinesis happens during late anaphase to telophase (Green *et al.*, 2012). In typical cytokinesis, anillin localizes to the nucleus during interphase and is recruited to the cell membrane during mitosis. When cellularization starts, however, anillin is immediately recruited to the nascent cleavage furrows, in contrast to a slower enrichment in the nucleus (Field *et al.*, 2005). An intriguing hypothesis is that the function of Dunk is required to adapt the behavior of anillin during the normal cell cycle to support cytokinesis during interphase. For example, because Dunk is predicted to bind to the conserved AH and PH domains of anillin, Dunk may work in synergy with RhoA and $PI(4,5)P_2$ to promote the localization of anillin to the cleavage furrows. Alternatively, Dunk may inhibit the nuclear entry of anillin by blocking its interaction with nuclear import receptors. Future research investigating these possibilities will help elucidate the molecular mechanism underlying the Dunk-mediated regulation of anillin and provide insight into how unique, cellularization-specific gene products interplay with conserved, common cellular machinery to facilitate a noncanonical form of cleavage.

MATERIALS AND METHODS

Request a protocol through *Bio-protocol*.

Yeast two-hybrid assay

Full-length *dunk* was cloned into pGBKT-7 plasmid (a vector containing DNA-BD of GAL4) and transformed into Y2H Gold yeast cell as the bait for all the yeast two-hybrid experiments (Y2HGold[pGBKT7-Dunk]). The expression of Dunk protein was confirmed by Western blot using c-Myc Monoclonal Antibody (Takara, Catalogue# 631206; See below for details). Then, the Y2HGold[pGBKT7-Dunk] was tested for autoactivation and toxicity. The results of the tests are described below. First, Y2Hgold[pGBKT7-Dunk] yeast colonies on the SDO/X plates were in white color, indicating that Dunk BD alone cannot activate the transcription of the reporter gene *MEL1*, whose product can hydrolyze colorless X-alpha-Gal into a product with

blue color. Second, Y2HGold[pGBKT7-Dunk] could not survive on SDO/X/A plates, indicating that Dunk BD alone cannot activate the transcription of the reporter gene *AUR1-C*, which is required for survival on the plates with Aureobasidin A. Finally, the growth of Y2HGold[pGBKT7-Dunk] cell was comparable to Y2HGold[pGBKT7], indicating the Dunk protein is not toxic when expressed in yeast.

To perform the screen for Dunk binding proteins, a full-length Dunk was used to screen the Mate & Plate Library - Universal *Drosophila* (Normalized; Takara, catalogue no. 630485). This genome-wide *Drosophila* cDNA library is prepared from equal quantities of poly-A^+ RNA isolated from embryo, larva and adult stage *Drosophila*, covering most of the expressed genes in *Drosophila*. The gene representation has been equalized by reducing the copy number of abundant cDNAs which in turn increased the occurrence of low copy number transcripts (Zhulidov *et al.*, 2004). This *Drosophila* cDNA library was cloned into pGADT-7 plasmid (a vector containing activation domain [AD] of GAL4) and transformed into yeast strain Y187. The screen was performed followed by the Matchmaker Gold Yeast Two-Hybrid System User Manual (Takara, 071519). One large Y2HGold[pGBKT7-Dunk] yeast colony was picked from a fresh SD/-Trp plate and inoculated into 50 ml of SD/-Trp liquid media. The culture was incubated and shook (250–270 rpm) at 30°C until the OD_{600} reaches 0.8 (16–20 h). Y2HGold[pGBKT7-Dunk] yeast cells were pelleted by centrifuging at 1000 g for 5 min. The pellet was resuspended to a cell density of gt 1×10^8 cells per ml in SD/–Trp (4–5 ml). The cell density of Y2HGold[pGBKT7-Dunk] was checked by the hemocytometer under the phase-contrast microscope. After checking the quality of the library strain by titering on SD/-Leu plates (1-ml library should contain more than 2×10^7 cells), 1 ml of the library strain was combined with the Y2HGold[pGBKT7-Dunk] strain in a sterile 2-l flask with 45-ml 2 × YPDA liquid medium (with 50-μg/ml kanamycin). The culture was incubated and shook at 30°C for 20 h at 50 rpm. The formation of the zygotes was checked under the phase-contrast microscope after 20 h, indicating the mating between the bait strain and the library strain. Then cells were pelleted by centrifuging at 1000 g for 10 min. The cell pellet was resuspended with 50-ml 0.5 × YPDA (with 50-μg/ml kanamycin) and centrifuged to pellet the cells again. The cell pellet was resuspended again with 10-ml 0.5 × YPDA (with 50-μg/ml kanamycin). The total volume (volume of media + volume of cell, total volume [TV]) of the media and the cells are measured. 200 μl of the culture was plated on per 150-mm DDO/X/A plate. The plates were incubated at 30°C for 3–5 d. At the same time, spread 100 μl of 1/10, 1/100, 1/1000, and 1/10,000 dilutions of the mated culture on DDO 100-mm agar plates and incubate at 30°C for 3–5 d. The numbers of screened colonies were calculated by the number of diploids that grew on the DDO plates (Num), TV, plating volume (PV) and the dilution factor (D). Numbers of screened colonies = Num × TV/(PV × D). No less than 1 million diploids should be screened.

After 3–5 d, positive colonies (blue colonies) from the DDO/X/A plates were picked, and the plasmids purified from these positive clones were sequenced using the sequencing primers for the pGADT-7 plasmid. We have repeated this genome-wide screen three times and in total seven positive colonies were identified and sequenced. All the prey plasmids in those positive colonies contained the C-terminal of *Drosophila* anillin (630–1212 a.a.).

For the control, pGBKT7-53 (encodes the Gal4 DNA-BD fused with murine p53) and pGBKT7-Lam (which encodes the Gal4 BD fused with lamin) constructs were transformed into Y2H Gold yeast cells. pGADT7-T (encodes the Gal4 AD fused with SV40 large T-antigen) vector was transformed into Y187 yeast cell. Because p53 and large T-antigen are known to interact in a yeast two-hybrid assay (Li & Fields, 1993; Iwabuchi *et al.* 1993), mating Y2HGold [pGBKT7-53] with Y187 [pGADT7-T] was treated as the positive control for the screen. Because lamin does not interact with T-antigen in a yeast two-hybrid assay, Y2HGold [pGBKT7-lam] with Y187 [pGADT7-T] was treated as the negative control for the screen.

For identifying Dunk BD on anillin, Scraps truncations ani_CT (592–1212 a.a.), ani_PH (1000–1212 a.a.), ani_CTΔPH (592–999 a.a.), ani_ND (592–819 a.a.) and ani_AHPH (820–1212 a.a.) were cloned into pGADT-7 plasmid and transformed into yeast strain Y187 as preys. The truncations were designed based on Scraps isoform A because this isoform has the same C-terminal sequence as the prey strain we found in the genome-wide screen. The different anillin truncations were tested for binding to full-length Dunk using yeast two-hybrid. For testing the binding between Dunk and anillin mutants, anillin PQ (ani_PQ, V1080S, P1116S) and anillin RS (ani_RS, V1080S, T1087I) mutants (Field *et al.*, 2005) were cloned into pGADT-7 plasmids and transformed into yeast strain Y187 as preys. After mating, diploids were spotted on both YPDA and the DDO/–Leu/–Trp/X-alpha-Gal agar plates with different dilutions (Figure 1D, Supplemental Figures S1 and S2A). The growth of colonies on the YPDA plate indicates the amount of live yeast cells. The appearance and the survival of the colonies on the DDO/–Leu/–Trp/X-alpha-Gal agar plate indicate the successful mating of the bait and prey yeast strains, and the intensity of the blue color of the colonies indicates the strength of the interaction between the prey and the bait proteins.

To determine the expression level of prey and bait proteins, the bait- and prey-yeast strains were first inoculated in the SDO/-Trp media or SDO/-Leu media. The overnight media were then inoculated into the fresh selective media and grew to OD600 = 0.8. Yeast cells from 3-ml culture were collected through the centrifuge, and 400-μl lysis buffer (62.5-mM Tris-Hcl/12.5% Glycerol/2% SDS/ 2.5% β-mercaptoethanol/25 mM NaN_3/1 mM phenylmethylsulfonyl fluoride/dash of Bromophenol Blue) was added into the yeast cells. Cells were lysed by bead beating and boiled at 65°C for 5 min. The cell lysis was then analyzed by Western Blot. Bait protein was detected by c-Myc Monoclonal Antibody (Takara, Catalogue no. 631206, unpublished data) and prey proteins were detected by HA antibody (Cell Signalling Technology, Catalogue no. 3724S; Supplemental Figure S1, A and B).

Fly stocks and genetics

Fly lines containing the following fluorescent markers were used: *UAS-GFP-anillin* (*UAS-GFP-scraps*; Silverman-Gavrila *et al.*, 2008), *Sqh-mCherry* (Martin *et al.*, 2009), *Sqh-GFP* (Royou *et al.*, 2002), and *anillin-mCherry* (endogenously tagged, this study, see below for details). The *Maternal-Tubulin-Gal4* line 67.15 ("*67*" and "*15*" refer to *Maternal-Tubulin-Gal4* on chromosome II and III, respectively; Hunter and Wieschaus, 2000) was used to drive the expression of GFP-anillin.

OreR embryos were used as a control for immunostaining experiments unless stated otherwise. The *dunk*^{1} P-element insertion mutant line, *P{SUPor-P}CG42748*^{KG09309} (Bellen *et al.*, 2004), was obtained from Bloomington *Drosophila* Stock Center.

The following crosses were made to generate (1) *ani*/+, (2) *dunk*^{1}/+, and (3) *ani*/*dunk*^{1} heterozygous mutant embryos (Figure 6; Supplemental Figure S4; *ani* = *scraps*). Note that *ani*^{PQ} and *Sqh-GFP* are the maternal genotype and *dunk* is the zygotic genotype. (1) Females from *ani*^{PQ}*/Cyo(II)*; *Sqh-GFP (III)* were crossed to *OreR* males to generate *ani*^{PQ}*/+ (II)*; *Sqh-GFP (III)/+* embryos. In these embryos, the amount of maternally deposited, functional anillin is expected to be 50% of those in wild-type embryos. (2) Females from *Sqh-GFP (III)*

were crossed to *dunk*^{1}*(II)* males to generate *dunk*^{1}*/+ (II)*; *Sqh-GFP (III)/+* embryos. In these embryos, the amount of zygotically expressed Dunk is expected to be 50% of those in wild-type embryos. (3) Females from *ani*^{PQ}*/Cyo(II)*; *Sqh-GFP (III)* were crossed to *dunk*^{1}*(II)* males to generate *dunk*^{1}*/ani*^{PQ} *(II)*; *Sqh-GFP (III)/+* embryos. In these embryos, the amount of maternally-deposited, functional anillin and the amount of zygotically expressed Dunk is expected to be 50% of those in wild-type embryos. The localization of Sqh-GFP is examined in these three types of embryos and the wild-type embryos.

The *dunk bnk* double-mutant embryos (Figure 7) were generated from the *dunk*^{1}; *Df(3R)*$^{tll\text{-}e}$/TM3 flies. A quarter of the embryos are expected to be *dunk*^{1}*/dunk*^{1}; *Df(3R)*$^{tll\text{-}e}$*/Df(3R)*$^{tll\text{-}e}$. *Df(3R)*$^{tll\text{-}e}$ contains a deletion that covers both *bnk* and the terminal gap gene *tll* (Schejter and Wieschaus, 1993). Tll regulates the expression of pair-rule genes in a stereotyped manner (Frasch and Levine, 1987). Thus, embryos homozygous for this deficiency can be identified by the immunostaining of the products of pair-rule genes, such as Even skipped (Eve).

For generating *anillin* mutant embryos, *ani*^{PQ}*/Cyo*; *Sqh-GFP* females were crossed to *ani*^{RS}*/Cyo*; *Sqh-GFP* males to generate *ani*^{PQ}*/ani*^{RS}; *Sqh-GFP* transheterozygous flies (Schupbach and Wieschaus, 1989). Embryos derived from these flies were used to examine Dunk localization (Figure 5; Supplemental Figure S3), myosin localization (Figures 10 and 11) or furrow ingression rate (Supplemental Figure S2) by immunostaining or live imaging. *ani*^{PQ}and *ani*^{RS}are maternal-effect alleles containing point mutations in the PH domain (Field *et al*., 2005).

For examining the colocalization of myosin and anillin (Figures 8 and 9; Supplemental Figure S5), *UAS-GFP-anillin (III)* females were crossed to males from the *Maternal-Tubulin-Gal4-15 sqh-mCherry (III)* to generate *UAS-GFP-anillin (III)/ Maternal-Tubulin-Gal4-15 sqh-mCherry (III)* flies. Embryos derived from these flies were used to examine the localization of anillin and myosin by live imaging.

For generating the endogenously tagged anillin-mCherry line, CRISPR-mediated gene editing was performed by WellGenetics using modified methods of Kondo and Ueda (2013). In brief, gRNA sequence GGCCTCGTACCTGAGTAAAC[GGG] was cloned into U6 promoter plasmid. Cassette mCherry-3 × P3-GFP, which contains mCherry, a floxed 3 × P3-GFP, and two homology arms were cloned into pUC57-Kan as donor template for repair. *scraps/CG2092*-targeting gRNAs and hs-Cas9 were supplied in DNA plasmids, together with donor plasmid for microinjection into embryos of control strain *w[1118]*. F1 flies carrying the selection marker of 3 × P3-GFP were further validated by genomic PCR and sequencing. CRISPR generated a break in *scraps/CG2092*, and the sequence containing the break was subsequently replaced by cassette mCherry-3 × P3-GFP through homology-directed repair. 3 × P3-GFP was then flipped out by Cre recombinase. After excision, only a 48-bp RE-loxP-CG-RE sequence is left, which encodes a 16 a.a. linker between mCherry and the protein of interest. The sequence of the RE-loxP-CG-RE linker is RSITSYNVCYTKLSAS. Finally, homozygous stock of anillin-mCherry was generated and the fluorescence signal in embryos was examined on a Nikon inverted spinning disk confocal microscope equipped with Andor W1 dual camera.

Embryo fixation, antibody staining, and imaging

Antibody staining against Zipper and neurotactin (Nrt) was performed on heat-fixed embryos (Figure 7; Supplemental Figure S6). All the other antibody staining experiments were performed on formaldehyde-fixed embryos (Figures 2, 3 and 5; Supplemental Figure S3). After fixation, the vitelline membrane was removed by shaking in heptane and methanol.

The procedure of embryo staining and imaging for Figures 3 and 7; Supplemental Figure S6 were as follows: embryos were blocked with 10% BSA in PBS and 0.1% Tween 20 and incubated with primary antibodies in PBT (PBS/0.1% BSA/0.1% Tween 20) overnight at 4°C. Secondary antibodies coupled to Alexa488, Alexa561, and Alexa647 were used at 1:500 (Invitrogen). Embryos were mounted in Aqua Poly Mount (Polysciences) for confocal imaging. Confocal images were collected on a Leica SP5 confocal microscope with a 63 ×/1.3 NA glycerine-immersion objective lens and a pinhole setting of one airy unit.

The procedure of embryo staining for Figures 2 and 5; Supplemental Figure S3 were as follows: embryos were washed in PBT (PBS/0.1% BSA/0.1% TritonX-100/0.01%AZIDE), blocked with Blocking buffer (PBS/10% BSA/0.1% TritonX-100/ 0.01% AZIDE), and incubated with primary antibodies in Dilution buffer (PBS/5% BSA/0.1% TritonX-100/ 0.01% AZIDE) overnight at 4°C. Then embryos were washed 4 × 10 min in PBT and incubated with secondary antibodies in dilution buffer for 1–2 h at room temperature (22–25°C) followed by DAPI staining. Secondary antibodies coupled to Alexa488, Alexa561, and/or Alexa647 were used at 1:500 (Invitrogen). Final wash 4 × 10 min in PTW + AZIDE (PBS/0.1% Tween20/ 0.01% AZIDE). Embryos were mounted in Aqua Poly Mount (Polysciences) for confocal imaging. Confocal images were collected at room temperature on a Nikon inverted spinning disk confocal microscope equipped with Andor W1 dual camera. A CFI Plan Apo Lambda 60 ×/1.40 WD 0.13 mm Oil Objective Lens was used for imaging.

Primary antibodies were diluted with the following dilutions: rabbit anti-Zipper 1:100; mouse monoclonal anti-Nrt 1:10 (BP 106, Developmental Studies Hybridoma Bank); rabbit anti-Scraps 1:1000 (gift of C. Field); mouse monoclonal anti-Pnut 1:10 (4C9H4, Developmental Studies Hybridoma Bank); rabbit polyclonal anti-mCherry 1:200 (Abcam, ab167453); rat monoclonal anti-Dunk 1:100 (He *et al*., 2016); rabbit polyclonal anti-GFP 1:500 (AB3080, EMD Millipore); guinea pig anti-Eve 1:500 (Kosman *et al*., 1998).

To investigate Dunk localization in *anillin* mutant embryos (Figure 2), wild-type embryos, and mutant embryos derived from *ani*^{PQ}*/ani*^{RS}; *Sqh-GFP* transheterozygous females were fixed and mixed in the same tube for immunostaining with anti-GFP, anti-Dunk and anti-Pnut antibodies following the protocol described above. Positive staining for Sqh-GFP was used for recognizing *anillin* mutant embryos.

Live imaging

To prepare embryos for live imaging, manually staged embryos were collected at room temperature (22–25°C) on agar plates, dechorionated in 50% bleach for 1–2 min, rinsed thoroughly with water, and transferred on a 35-mm MatTek glass-bottom dish (MatTek). Distilled water was then added to the dish well to completely cover the embryos. To analyze furrow ingression rate, live imaging of wild-type and *anillin* mutant embryos was performed at room temperature on a Nikon Eclipse 90i Motorized Upright Fluorescence Microscope using 40 ×/0.80 water immersion objective lens under the DIC mode (Supplemental Figure S2). Fluorescence live imaging of basal myosin ring closure was performed on an Olympus FVMPE-RS multiphoton system with a 25 ×/1.05 numerical aperture water immersion objective lens (Supplemental Figure S7). All other fluorescence live-imaging experiments were performed at room temperature on a Nikon inverted spinning disk confocal microscope equipped with Andor W1 dual camera, dual-spinning disk module. A CFI Plan Apo Lambda 60 ×/1.40 WD 0.13 mm Oil Objective Lens was used for imaging. GFP- and mCherry-tagged proteins were imaged with a 488-nm laser and a 561-nm laser, respectively.

Image analysis and quantification

To compare myosin fluorescence intensity at the edges and vertices (Figure 10), the Sqh-GFP movies were analyzed using MATLAB (Image Processing Toolbox, The MathWorks; Natick, MA) as follows. First, maximum intensity projections were generated from raw images from seven adjacent confocal slices (0.5-μm z-step, ~ 3 μm thick) that cover the invagination front. Second, the projected images were subject to image background subtraction. Third, to define signals that belong to edges versus vertices, the basal outline of the cells (as marked by Sqh-GFP) was segmented using a MATLAB-based software package Embryo Development Geometry Explorer (EDGE; Gelbart *et al.*, 2012). In EDGE, the outlines of individual cells are represented by polygons and tracked over time. Along each polygon, we define points less than 1.2 μm away from the nearest vertex as "vertex", whereas points more than 1.2 μm away from the nearest vertex as "edge." Mean intensity was integrated at vertices and edges along with the corresponding line segments with a width of 0.3 μm. The median pixel intensity of the image is used as a proxy for the intensity of the cytoplasmic Sqh-GFP signal and is subtracted from the mean vertex and edge intensities. Finally, the intensity was normalized between embryos according to the median pixel intensity of the image.

To compare myosin puncta fluorescence intensity in wild-type and *anillin* mutant embryos (Figure 11), the Sqh-GFP movies were analyzed using MATLAB as follows. First, the maximum intensity projections were generated from raw images from five adjacent confocal slices (0.5-μm z-step, ~ 2.5 μm thick) that covered the most apical cortex. Second, the median pixel intensity of the image was used as a proxy for the intensity of the cytoplasmic Sqh-GFP signal and was subtracted from the entire image. The intensity was normalized between embryos according to the median pixel intensity of the image. Then, we randomly selected 20 discrete, representative apical-myosin puncta and measured their average intensity (Int_p). Finally, the number of pixels that had an intensity value larger than Int_p was quantified as a proxy for the total amount of apical myosin puncta.

To measure the rate of basal myosin ring closure (Supplemental Figure S7), the maximum projection of a 7-μm substack covering the furrow canals was generated for each time point using a custom MATLAB script. For each embryo, six myosin rings were randomly selected from the projection view, and the area of these rings was measured at T = 30, 36, 42, 48, and 54 min after the onset of cellularization. Eight wild-type and nine *dunk* mutant embryos were analyzed. The rate of ring closure was then calculated by dividing the change in area by the elapsed time.

Statistics

Statistical comparisons were performed using two-tailed Student's *t* tests. Sample sizes can be found in figure legends. *p* values were calculated using MATLAB ttest2 function (Two-tailed Student's *t* test).

ACKNOWLEDGMENTS

We thank Melissa Wang, Min Hur, and Amanda Socha for their help with the yeast two-hybrid experiments. We thank Ann M. Lavanway for her help with microscopy. We thank all the members of the Molecular Interactions & Imaging Core at the Institute for Biomolecular Targeting (bioMT) of Dartmouth College. We thank E. Wieschaus, T. Schupbach, A. Wilde, C. Field, and J. Moseley for sharing the reagents. We thank the laboratories of Guerinot ML, Bezanilla M and Barlowe C for sharing the yeast two-hybrid strains and the protocol for making yeast lysates. We thank the Bloomington *Drosophila* Stock Center (NIH-P40OD018537) for providing fly stocks used in this study. We thank all members of the He lab and Griffin lab for helpful discussions. This research is supported by National Institute of General Medical Sciences ESI-MIRA (R35GM128745) and the start-up fund to B.H. The study used core services supported by STANTO15R0 (CFF RDP), P30-DK117469 (NIDDK P30/DartCF), and P20-GM113132 (bioMT COBRE).

REFERENCES

Acharya S, Laupsien P, Wenzl C, Yan S, Großhans J (2014). Function and dynamics of slam in furrow formation in early Drosophila embryo. Dev Biol 386, 371–384.

Adam JC, Pringle JR, Peifer M (2000). Evidence for functional differentiation among Drosophila septins in cytokinesis and cellularization. Mol Biol Cell 11, 3123–3135.

Afshar K, Stuart B, Wasserman SA (2000). Functional analysis of the Drosophila diaphanous FH protein in early embryonic development. Development 127, 1887–1897.

Arnold TR, Shawky JH, Stephenson RE, Dinshaw KM, Higashi T, Huq F, Davidson LA, Miller AL (2019). Anillin regulates epithelial cell mechanics by structuring the medial-apical actomyosin network. eLife 8, e39065.

Bellen HJ, Levis RW, Liao G, He Y, Carlson JW, Tsang G, Evans-Holm M, Hiesinger PR, Schulze KL, Rubin GM, *et al.* (2004). The BDGP gene disruption project: single transposon insertions associated with 40% of Drosophila genes. Genetics 167, 761–781.

Budnar S, Husain KB, Gomez GA, Naghibosadat M, Varma A, Verma S, Hamilton NA, Morris RG, Yap AS (2019). Anillin promotes cell contractility by cyclic resetting of RhoA residence kinetics. Dev Cell 49, 894–906.e12.

Crawford JM, Harden N, Leung T, Lim L, Kiehart DP (1998). Cellularization in Drosophila melanogaster is disrupted by the inhibition of rho activity and the activation of Cdc42 function. Dev Biol 204, 151–164.

Cui Z, Mo J, Song P, Wang L, Wang R, Cheng F, Wang L, Zou F, Guan X, Zheng N, *et al.* (2022). Comprehensive bioinformatics analysis reveals the prognostic value, predictive value, and immunological roles of ANLN in human cancers. Front Genet 13, 1000339.

DeBiasio RL, LaRocca GM, Post PL, Taylor DL (1996). Myosin II transport, organization, and phosphorylation: evidence for cortical flow/solation-contraction coupling during cytokinesis and cell locomotion. Mol Biol Cell 7, 1259–1282.

Eggert US, Mitchison TJ, Field CM (2006). Animal cytokinesis: from parts list to mechanisms. Annu Rev Biochem 75, 543–566.

Field CM, Alberts BM (1995). Anillin, a contractile ring protein that cycles from the nucleus to the cell cortex. J Cell Biol 131, 165–178.

Field CM, Coughlin M, Doberstein S, Marty T, Sullivan W (2005). Characterization of anillin mutants reveals essential roles in septin localization and plasma membrane integrity. Development 132, 2849–2860.

Foe VE, Alberts BM (1983). Studies of nuclear and cytoplasmic behaviour during the five mitotic cycles that precede gastrulation in Drosophila embryogenesis. J Cell Sci 61, 31–70.

Frasch M, Levine M (1987). Complementary patterns of even-skipped and fushi tarazu expression involve their differential regulation by a common set of segmentation genes in Drosophila. Genes Dev 1, 981–995.

Fullilove SL, Jacobson AG (1971). Nuclear elongation and cytokinesis in Drosophila montana. Dev Biol 26, 560–577.

Gelbart MA, He B, Martin AC, Thiberge SY, Wieschaus EF, Kaschube M (2012). Volume conservation principle involved in cell lengthening and nucleus movement during tissue morphogenesis. Proc Natl Acad Sci USA 109, 19298–19303.

Green RA, Paluch E, Oegema K (2012). Cytokinesis in animal cells. Annu Rev Cell Dev Biol 28, 29–58.

Grosshans J, Wenzl C, Herz HM, Bartoszewski S, Schnorrer F, Vogt N, Schwarz H, Müller HA (2005). RhoGEF2 and the formin Dia control the formation of the furrow canal by directed actin assembly during Drosophila cellularisation. Development 132, 1009–1020.

He B, Martin A, Wieschaus E (2016). Flow-dependent myosin recruitment during drosophila cellularization requires zygotic dunk activity. Development 143, 2417–2430.

Hunter C, Wieschaus E (2000). Regulated expression of nullo is required for the formation of distinct apical and basal adherens junctions in the drosophila blastoderm. J Cell Biol 150, 391–401.

Kosman D, Small S, Reinitz J (1998). Rapid preparation of a panel of polyclonal antibodies to drosophila segmentation proteins. Dev Genes Evol 208, 290–294.

Krueger D, Quinkler T, Mortensen SA, Sachse C, De Renzis S (2019). Cross-linker-mediated regulation of actin network organization controls tissue morphogenesis. J Cell Biol 218, 2743–2761.
Lecuit T, Samanta R, Wieschaus E (2002). Slam encodes a developmental regulator of polarized membrane growth during cleavage of the drosophila embryo. Dev Cell 2, 425–436.
Liang HL, Nien CY, Liu HY, Metzstein MM, Kirov N, Rushlow C (2008). The zinc-finger protein Zelda is a key activator of the early zygotic genome in Drosophila. Nature 456, 400–403.
Liu J, Fairn GD, Ceccarelli DF, Sicheri F, Wilde A (2012). Cleavage furrow organization requires PIP(2)-mediated recruitment of anillin. Curr Biol 22, 64–69.
Martin AC, Kaschube M, Wieschaus EF (2009). Pulsed contractions of an actin-myosin network drive apical constriction. Nature 457, 495–499.
Mason FM, Xie S, Vasquez CG, Tworoger M, Martin AC (2016). RhoA GTPase inhibition organizes contraction during epithelial morphogenesis. J Cell Biol 214, 603–617.
Mazumdar A, Mazumdar M (2002). How one becomes many: blastoderm cellularization in Drosophila melanogaster. Bioessays 24, 1012–1022.
Merrill PT, Sweeton D, Wieschaus E (1988). Requirements for autosomal gene activity during precellular stages of Drosophila melanogaster. Development 104, 495–509.
Naydenov NG, Koblinski JE, Ivanov AI (2021). Anillin is an emerging regulator of tumorigenesis, acting as a cortical cytoskeletal scaffold and a nuclear modulator of cancer cell differentiation. Cell Mol Life Sci 78, 621–633.
Normand G, King RW (2010). Understanding cytokinesis failure. Adv Exp Med Biol 676, 27–55.
Barmchi MP, Rogers S, Hacker U (2005). DRhoGEF2 regulates actin organization and contractility in the Drosophila blastoderm embryo. J Cell Biol 168, 575–585.
Piekny AJ, Glotzer M (2008). Anillin is a scaffold protein that links RhoA, actin, and myosin during cytokinesis. Curr Biol 18, 30–36.
Piekny AJ, Maddox AS (2010) The myriad roles of Anillin during cytokinesis. Semin Cell Dev Biol 21, 881–891.
Pollard TD, O'Shaughnessy B (2019). Molecular mechanism of cytokinesis. Annu Rev Biochem 88, 661–689.
Rappaport R (1971). Cytokinesis in animal cells. Int Rev Cytol 31, 169–213.
De Renzis S, Elemento O, Tavazoie S, Wieschaus EF (2007). Unmasking activation of the zygotic genome using chromosomal deletions in the Drosophila embryo. PLoS Biol 5, e117.
Reversi A, Loeser E, Subramanian D, Schultz C, De Renzis S (2014). Plasma membrane phosphoinositide balance regulates cell shape during Drosophila embryo morphogenesis. J Cell Biol 205, 395–408.
Rose LS, Wieschaus E (1992). The Drosophila cellularization gene nullo produces a blastoderm-specific transcript whose levels respond to the nucleocytoplasmic ratio. Genes Dev 6, 1255–1268.
Royou A, Field C, Sisson JC, Sullivan W, Karess R (2004). Reassessing the role and dynamics of nonmuscle myosin II during furrow formation in early Drosophila embryos. Mol Biol Cell 15, 838–850.
Royou A, Sullivan W, Karess R (2002). Cortical recruitment of nonmuscle myosin II in early syncytial Drosophila embryos: its role in nuclear axial expansion and its regulation by Cdc2 activity. J Cell Biol 158, 127–137.
Schejter ED, Wieschaus E (1993). Bottleneck acts as a regulator of the microfilament network governing cellularization of the Drosophila embryo. Cell 75, 373–385.
Schupbach T, Wieschaus E (1989). Female sterile mutations on the second chromosome of Drosophila melanogaster. I. Maternal effect mutations. Genetics 121, 101–117.
Schweisguth F, Lepesant JA, Vincent A (1990). The serendipity alpha gene encodes a membrane-associated protein required for the cellularization of the Drosophila embryo. Genes Dev 4, 922–931.
Sharma S, Rikhy R (2021). Spatiotemporal recruitment of RhoGTPase protein GRAF inhibits actomyosin ring constriction in Drosophila cellularization. eLife 10, e63535.
Shimizu S, Seki N, Sugimoto T, Horiguchi S, Tanzawa H, Hanazawa T, Okamoto Y (2007). Identification of molecular targets in head and neck squamous cell carcinomas based on genome-wide gene expression profiling. Oncol Rep 18, 1489–1497.
Silverman-Gavrila RV, Hales KG, Wilde A (2008). Anillin-mediated targeting of peanut to pseudocleavage furrows is regulated by the GTPase Ran. Mol Biol Cell 19, 3735–3744.
Sokac AM, Biel N, De Renzis S (2023). Membrane-actin interactions in morphogenesis: lessons learned from Drosophila cellularization. Semin Cell Dev Biol 133, 107–122.
Sokac AM, Wieschaus E (2008). Zygotically controlled F-actin establishes cortical compartments to stabilize furrows during Drosophila cellularization. J Cell Sci 121, 1815–1824.
Sun L, Guan R, Lee IJ, Liu Y, Chen M, Wang J, Wu JQ, Chen Z (2015). Mechanistic insights into the anchorage of the contractile ring by anillin and Mid1. Dev Cell 33, 413–426.
Tadros W, Lipshitz HD (2009). The maternal-to-zygotic transition: a play in two acts. Development 136, 3033–3042.
Thomas JH, Wieschaus E (2004). src64 and tec29 are required for microfilament contraction during Drosophila cellularization. Development 131, 863–871.
Uehara R, Goshima G, Mabuchi I, Vale RD, Spudich JA, Griffis ER (2010). Determinants of myosin II cortical localization during cytokinesis. Curr Biol 20, 1080–1085.
Wang D, Chadha GK, Feygin A, Ivanov AI (2015). F-actin binding protein, anillin, regulates integrity of intercellular junctions in human epithelial cells. Cell Mol Life Sci 72, 3185–3200.
Wenzl C, Yan S, Laupsien P, Grosshans J (2010). Localization of RhoGEF2 during Drosophila cellularization is developmentally controlled by Slam. Mech Dev 127, 371–384.
Wieschaus E, Sweeton D (1988). Requirements for X-linked zygotic gene activity during cellularization of early Drosophila embryos. Development 104, 483–493.
Xue Z, Sokac AM (2016). Back-to-back mechanisms drive actomyosin ring closure during Drosophila embryo cleavage. J Cell Biol 215, 335–344.
Yumura S, Ueda M, Sako Y, Kitanishi-Yumura T, Yanagida T (2008). Multiple mechanisms for accumulation of myosin II filaments at the equator during cytokinesis. Traffic 9, 2089–2099.
Zhang L, Wei Y, He Y, Wang X, Huang Z, Sun L, Chen J, Zhu Q, Zhou X (2023). Clinical implication and immunological landscape analyses of ANLN in pan-cancer: A new target for cancer research. Cancer Med 12, 4907–4920.
Zheng L, Sepúlveda LA, Lua RC, Lichtarge O, Golding I, Sokac AM (2013). The maternal-to-zygotic transition targets actin to promote robustness during morphogenesis. PLoS Genet 9, e1003901.
Zhulidov PA, Bogdanova EA, Shcheglov AS, Vagner LL, Khaspekov GL, Kozhemyako VB, Matz MV, Meleshkevitch E, Moroz LL, Lukyanov SA, Shagin DA (2004). Simple cDNA normalization using kamchatka crab duplex-specific nuclease. Nucleic Acids Res 32, e37.